NASA Technical Memorandum 104577

Modulation Characteristics of a High–Power Semiconductor Master Oscillator Power Amplifier (MOPA)

Donald Mitchell Cornwell, Jr.
NASA Goddard Space Flight Center
Greenbelt, Maryland

National Aeronautics and
Space Administration

Goddard Space Flight Center
Greenbelt, Maryland 20771

1992

Thesis submitted to the Faculty of the Graduate School of
The University of Maryland in partial fulfillment
of the requirements for the degree of
Master of Science
1991

ACKNOWLEDGEMENTS

I would like to acknowledge Professor Christopher C. Davis and Mr. Robert K. Zimmerman for many helpful discussions in reference to this research. I would like to acknowledge Dr. Michael A. Krainak and Mr. Bernard D. Seery, whose full support I have enjoyed for an admirably long amount of time. I would also like to acknowledge Ms. Camilla Keis Hansen, who managed to put up with me during this time.

Advisory Committee:

Professor Christopher C. Davis, Chairman/Advisor
Professor Ping-Tong Ho
Professor Mario Dagenais

TABLE OF CONTENTS

LIST OF TABLES

LIST OF FIGURES

LIST OF FIGURES

LIST OF FIGURES

Introduction

Semiconductor diode lasers are capable of producing high optical output powers (currently up to 10 Watts CW [1]) from relatively small packages as compared to other lasers. Low power (<100 mW) diode lasers are used extensively in current optical fiber communication systems. The size and efficiency of diode lasers make them attractive for many spaceborne applications such as free-space laser communication, LIDAR, and laser ranging and altimetry. Unfortunately, the high power versions of these devices exhibit properties which limit their abilities in such applications. These properties include multimode far-field radiation patterns and multi-longitudinal mode spectra. All of these applications require a high-power (>200 mW average) modulated beam which exhibits a single-mode, diffraction-limited radiation pattern and a single longitudinal-mode spectrum.

A significant portion of the current research in the area of high power semiconductor lasers is focused on techniques to achieve single-mode spatial and spectral beam quality. One technique that has been demonstrated to produce a high-power, diffraction-limited beam is to use a high-power semiconductor laser to amplify the beam of a low-power, diffraction-limited laser, where the high-power laser has been anti-reflection (AR) coated to eliminate self-oscillation or lasing. This technique is commonly known as a master oscillator-power amplifier (or MOPA) configuration, and the result is a high-power beam (450 mW cw [2]) with most of the power contained in a near-diffraction-limited spatial lobe and at the same frequency as the master oscillator.

The objective of our research is to design and build a semiconductor AlGaAs MOPA and then evaluate its performance when the beam of the master oscillator is modulated. The power amplifier in this case is an AR-coated AlGaAs broad area laser (BAL); the master oscillator is a single-mode index-guided AlGaAs laser. The small-signal and large-signal modulation behavior of the MOPA will be evaluated and compared to the behavior predicted by a reflective Fabry-Perot amplifier model of the broad area laser.

Diffraction-limited amplification of a beam from a master oscillator was initially observed while injecting it into high-power gain-guided AlGaAs semiconductor lasers arrays [3-4]. These devices also have broad emission areas, but diffraction-limited output from the injected array was also observed when the device was biased above its own oscillation threshold. Based on this observation, the diffraction-limited output beam was initially attributed to the frequency- and phase-locking of the individual array elements to the single-frequency master oscillator - a technique known as "injection locking"- which caused the elements to oscillate with a common phase and resulted in a single-lobed superposition of the far-field patterns of the individual elements [5-7].

When single-mode behavior was also observed from injected broad area lasers, an alternate theory was proposed which described an injected broad-area device (including semiconductor laser arrays) as a resonant regenerative Fabry-Perot amplifier operating in the strongly-saturated gain region [8]. The single lobe in the far-field is the result of the superposition of many off-axis, coherent passes of the master oscillator beam, which are amplified as they propagate through the device. Observed beamsteering and changes in the power of the single lobe due to changes in injected wavelength are also explained using this model of the device.

This Fabry-Perot amplifier (FPA) model is used as the basis of our research. The theoretical model is first incorporated into a program on a personal computer, and then is used to design an optical configuration which optimally couples light from the master oscillator laser into the amplifier. As an initial experiment, the far-field pattern, near-field pattern, spectrum, locking bandwidth and gain of the injected amplifier are characterized as a function of cw injection power and wavelength for amplifier bias current levels set both below and above the oscillation threshold. The properties of the amplified output for cw injection are then compared to those predicted by the computer-based Fabry-Perot amplifier model.

The amplified beam properties are then characterized by the condition of the modulated master oscillator, where the intensity is modulated by switching the bias current to the laser. It is well-documented that the intensity modulation (AM) of a semiconductor laser will also produce a spurious frequency modulation (FM) of the laser output [9], which is commonly known as "frequency chirp." A knowledge of the AM and FM properties of the master oscillator is required to understand their ensuing effects on the overall modulation performance of the MOPA. It is therefore required that the small-signal AM and FM frequency response of the master oscillator be characterized, which is conducted using a network analyzer and a scanning Fabry-Perot interferometer, respectively.

The small-signal AM frequency response of the injected BAL is then characterized for AM/FM modulation of the master oscillator. The AM response of the amplifier is compared to the predicted response, in order to determine the validity of the FPA model under modulated conditions. In addition, the results of the small-signal analysis are used to predict the large-signal, AM square-wave modulation behavior of the injected BAL, by Fourier-transforming the frequency response to calculate the step impulse response of the amplifier. The behavior of the amplifier is subsequently characterized for AM square-wave modulation (50% duty-cycle) of the master oscillator at modulation frequencies of 10 MHz and 250 MHz. The small-signal AM and square-wave modulation analyses are carried out for BAL bias currents of $0.95I_{th}$ (70 mW free-running) and $1.4I_{th}$ (530 mW) when the MO is biased for 50 mW of average power, which is the maximum average power for square-wave modulation that can be achieved by our drive electronics.

The overall behavior of the MOPA under modulated injection is assessed and compared to the results predicted by the reflective FPA model of the injected BAL.

Section 1: Background

1.1 Review of Previous Work

The size and efficiency of semiconductor lasers make them an extremely attractive source for many applications such as free-space optical communications, laser ranging, and altimetry. These applications all require diffraction-limited beams with several hundred milliwatts to several watts of optical power. Because of the internal power densities involved, the generation of high output power from a semiconductor laser requires a broad emission area. Unfortunately, the broad size of the waveguide reduces the oscillation threshold for the high order waveguide modes, resulting in multi-mode operation and a subsequent dual-lobed intensity distribution in the far-field. Semiconductor lasers which support only single transverse mode operation are typically limited in output power to 150 mW [10].

In theory, a diffraction-limited beam with cw power greater than 150 mW may be generated by passing a low power beam through an ideal region of gain, where the ideal gain region does not introduce any spatial aberration to the beam. This gain block is commonly known as a laser amplifier. Laser amplifiers based on III-V semiconductors have been successfully demonstrated by numerous researchers in the field of optical fiber communication [11,12]. These devices are fabricated by anti-reflection (AR) coating the front and rear facets of a semiconductor laser with a dielectric, in order to destroy the self-oscillation which would normally occur due to the optical feedback from the facets. The semiconductor laser amplifier used in optical fiber communications is typically a single-mode waveguide device; therefore most theoretical models of these devices are one dimensional; i.e., they assume that there are no transverse variations in the beam. The most current models of these devices are successful in describing most aspects of their behavior, including the dynamic behavior of the semiconductor amplifier under modulated injection [13,14]. In the section to follow, we will present a cursory discussion of one-dimensional semiconductor laser amplifier theory as it relates to our problem.

In reality, semiconductor laser amplifiers have shown limited success, due primarily to the coupling losses into the single-mode waveguide, and also due to the residual reflectivities of the facets. The best anti-reflection coatings achieved have been reported to be $r < 10^{-4}$ [15], which still results in frequency sensitivity due to residual Fabry-Perot resonances and also self-oscillation at a certain level of gain. Cleaving the facets of the device at slight angles has also been used to reduce the feedback from the facets [16]. The Fabry-Perot resonances of the cavity have also been noted to shift with carrier density due to a change in the internal index of refraction with carrier density [37,38].

It must be noted that all of the semiconductor laser amplifier research in the fiber community has been based on single-mode devices, which suffer the same basic cw power limitations as single-mode lasers. In order to reach higher gains (and higher internal photon densities), multi-mode devices, such as broad area lasers, must be used. The initial experiments with these devices saw them used as single-pass, travelling wave amplifiers (TWA), much like the amplifiers used in fiber communications. Unfortunately, the amplified beams from these devices exhibit transverse "filamentation" and other spatial aberrations which are caused by spatial hole burning due to gain saturation. These aberrations limit the use of travelling wave broad area amplifiers in applications requiring diffraction-limited power [17].

The first experiments to successfully demonstrate a high-power, diffraction-limited beam from an injected broad area semiconductor device were reported by Goldberg, et al. [3] and Hohimer, et al. [4] in 1985. These experiments were actually performed using AlGaAs semiconductor laser arrays rather than broad area lasers. A semiconductor laser array (see Figure 1.1) is a broad area device which has been proton-bombarded with stripes of high-resistance material, which in turn channel the current between the stripes and through the active region of the device. This localization of current causes lasing to occur in discrete regions which are known as array elements. These elements typically do not lase in phase with each other, and the resulting radiation pattern has the undesirable quality of multiple lobes in the far-field.

Goldberg, et al. [3], reported 100 mW of power in a single lobe with a width of 0.5° FWHM when the array was injected at a slight angle (3° to 5°) to the front facet. The single lobe was emitted from the front facet at an angle opposite to the injection angle(-3° to -5°), which is similar to the operation of the device as a reflective Fabry-Perot amplifier. The spectrum of the power in the single mode was measured to be single frequency, with the same frequency as the master oscillator. The angle of the single lobe was observed to steer

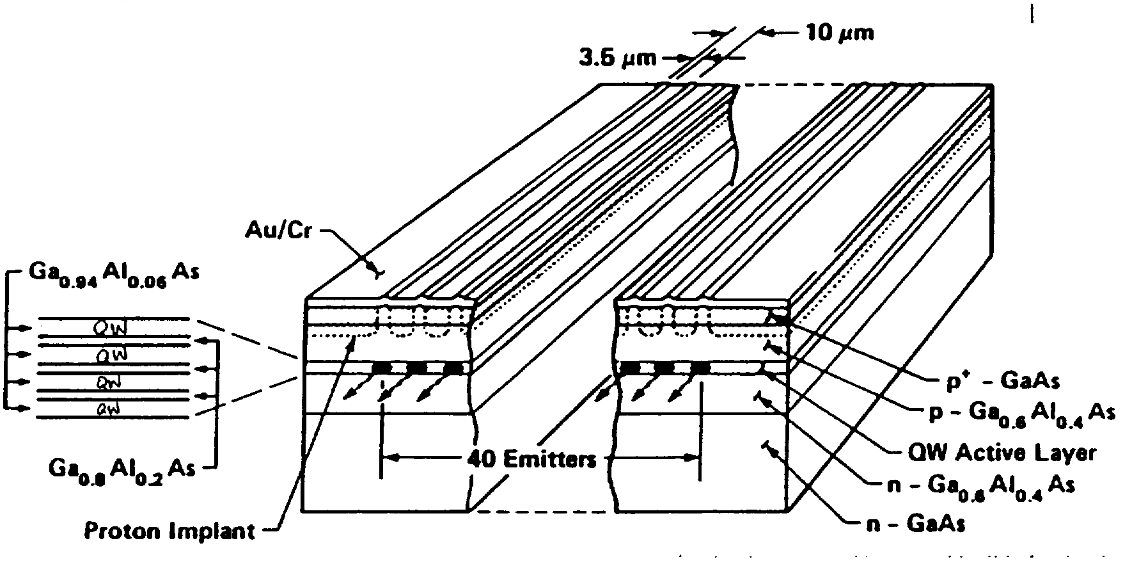

Figure 1.1 Schematic of basic structure of gain-guided semiconductor laser array [Referenced from Spectra Diode Laboratories, San Jose, CA].

when the wavelength of the injection source, or master laser, was changed. The amplitude of the single lobe was also observed to change with injected wavelength, giving rise to a locking bandwidth for the device which is defined as the frequency tuning range over which the amplitude of the single lobe is greater than 50% of the peak amplitude. The locking bandwidth was also discovered to be a function of the injected power.

Later research pushed the highest diffraction-limited power in the single lobe to 450 mW cw from a 600 mW device [2], with measured small-signal gains of up to 23 dB. A two-stage configuration has also been reported [18] which generated cw diffraction-limited beams up to 510 mW with small-signal gains of

25 dB and saturated signal gains of 14 dB. More recent experiments have demonstrated 2.6 W [19] and 12 W [20] of diffraction-limited power under pulsed conditions (0.5 μs pulses, 10% duty-cycle) under strong injection for P_{in}=365 mW and P_{in}=500 mW, respectively. Each forementioned case demonstrated the same properties of optimum output for off-axis injection, beamsteering, and amplitude changes for changes in the injected wavelength.

The observed single mode operation of injected semiconductor laser arrays was initially attributed to injection locking [3]. As was mentioned previously, the multi-mode far-field pattern typical of semiconductor laser arrays is attributable to the non-zero phase difference between the individual oscillator elements of the array [21]. In injection locking theory, some fraction of the injected beam falls incident on each of the array elements by proper shaping of the beam. Each element then becomes frequency- and phase-locked to the external oscillator signal, as has been observed in other systems [5,6], including semiconductor lasers [7]. All of the elements are now phase-locked to the same source, implying a common phase (and a zero phase difference) between them. This zero phase difference results in the constructive superposition of the fields emitted from each element, which in turn results in a single-lobe intensity pattern in the far-field [21].

This model was capable of explaining the single mode behavior of the device, but it could not explain the beamsteering behavior observed when detuning the frequency of the master oscillator [22]. A more complex version of the injection locking model has recently been introduced which successfully explains these phenomena in injected semiconductor laser arrays [23].

An alternative model to the injection locking approach was developed based on the results of off-axis injection experiments with a broad area laser [8]. These experiments revealed that an injected broad area laser demonstrated the exact same behavior as an injected semiconductor laser array. This results suggested that both the broad area laser and the injection-locked array were better described as reflective Fabry-Perot amplifiers which are operated in the highly-regenerative region. The far-field behavior of the injected device is explained based on a two-dimensional model of transverse Gaussian beam propagation through a large optical cavity. The gain of the cavity, including front and rear facet losses, is assumed to be uniformly saturated to a value of 1. The emitted field pattern is the superposition of many passes of the injected, off-axis Gaussian beam, which is amplified while simultaneously reducing the gain for the free-running modes of the device. This simple model is capable of explaining all of the observed far-field effects, including the single-lobed behavior and beamsteering with change in injected frequency. In addition, the model is successful in determining the optimum injection parameters for the device, such as injected spot size and injection angle. A more detailed discussion of this model will be presented in Section 1.2.

The two-dimensional reflective Fabry-Perot amplifier makes one assumption: that the gain of the device is uniformly saturated to unity. In actuality, the gain is non-linear as a function of injected intensity; in addition, the propagation of the beam through the device does not uniformly saturate the gain, leading to spatial hole burning and transverse gain variation. By the Kramers-Kronig relations, this variation in gain results in an inhomogeneous index variation, which in turn introduces spatial and temporal phase aberrations in the beam as it propagates through the device. Models which incorporate non-linear gain and index variations have been developed, but basically they involve numerical solutions which require computing power on the order of a supercomputer [24,25]. The injected amplifier behavior calculated from these models does not differ significantly from the simple Fabry-Perot amplifier model, which verifies that the assumption of uniform, unity gain is valid to first order.

It must be noted that none of the existing two-dimensional amplifier models deal with dynamic or time-varying effects, and very few experiments have been conducted on the modulated behavior of these devices. The locking bandwidth feature of injection-locking has been used to measure the FM modulation response of a semiconductor laser array [26]. An injection-locked array has also been used to demonstrate high-speed beamsteering by frequency modulation of the array [27]. Experiments involving high-power coherent communication with injected broad area devices have also been reported, with 310 mW of diffraction-limited power produced at 110 Mbps FSK modulation [28], and 120 mW of diffraction-limited power produced for 1 Gbps DPSK modulation [29]. No experiments have yet been reported which involve the amplitude modulation (AM) behavior of an injected broad area semiconductor laser amplifier.

The previous few pages have served as a general review of the past work which leads up to our amplitude-modulated (AM) injection experiments for a broad area semiconductor laser. The diffraction-limited far-field behavior of these devices can be described based on a two-dimensional model of the broad area device as a reflective Fabry-Perot amplifier, although this model is limited to some basic assumptions about the gain of the device. Although one-dimensional dynamic models of these devices have been developed by the optical fiber communications community, there are currently no two-dimensional models for broad area devices which incorporate dynamical or time-dependent behavior.

1.2 Two-Dimensional Reflective Fabry-Perot Amplifier Model

The unique diffraction-limited performance of the injected broad area laser is attributable to the two-dimensional qualities of the device when modelled as a reflective Fabry-Perot amplifier. The two-dimensional Fabry-Perot amplifier model as presented by Abbas, et al. [8] describes the transverse mode injection behavior of a broad area laser in terms of Gaussian beam propagation through a large optical cavity. The general concept of the two-dimensional model is shown in Figure 1.2. The master oscillator beam is focused to a waist at one end along the width of the BAL with an incidence angle which is a few degrees off of the facet normal. The injected beam is refracted and then propagates through the device to the high-reflectivity rear facet, where it is reflected back through the

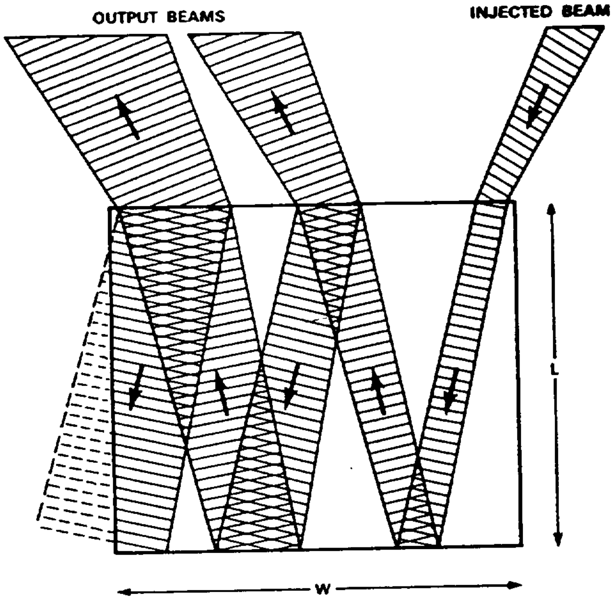

Figure 1.2: Fabry-Perot model for a broad area laser with injection. A Gaussian beam is emitted after each pass through the device. The internal beam is attenuated without reflection at the left edge of the device. L=500 µm. W=400 µm. (From Reference [8]*).*

device to the partially-reflecting front facet. At the front facet, most of the beam will be coupled out of the device, but a residual amount will be reflected back into the broad area laser. Although the reflected power is small, the small-signal gain in the device is high enough so that the gain quickly saturates, and the intensity of the beam from the second pass is soon comparable to the intensity of the beam from the first pass. The largest fraction of the second pass is again coupled out of the BAL, and the residual power will continue to propagate and be amplified in the device for many more passes. The model assumes that there are no reflections from the right or left edges of the gain region. The output of the injected BAL is then the superposition of the delayed and offset Gaussian beam emitted from each pass, and the intensity pattern in the far-field will consist of an angularly-offset single lobe if spatial coherence is maintained for each pass through the device.

Two initial assumptions are made about the broad area laser; namely, that the gain of the cavity, including mirror losses, is fully saturated to a value of unity, and that no index inhomogeneities exist in the device. This second assumption simplifies the problem by eliminating the effects of thermal lensing and spatial hole burning due to gain saturation, an assumption which is valid for low bias levels of the device.

The following mathematical treatment for the two-dimensional Fabry-Perot amplifier model is taken directly from Reference [8]. Figure 1.3 shows a detailed schematic of the initial pass of the injected beam through the BAL, as viewed from above. The coordinate system has been defined such that the *z*-axis runs along

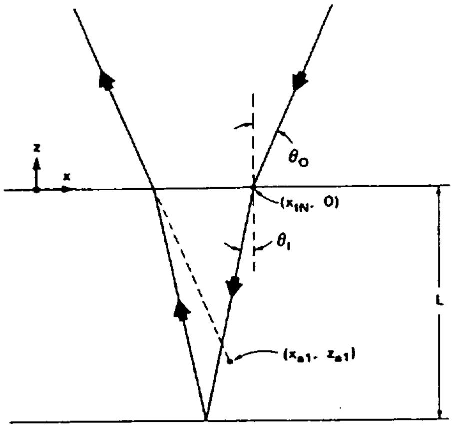

Figure 1.3: Schematic diagram showing the operation of a Fabry-Perot cavity on an injected beam. The parameters are described in the text (From Reference [8]*).*

the length of the device, while the x-axis lies along the width of the device. Variation along the y-axis (into the page) can be ignored, since the beam is guided along this axis and does not diverge. The master oscillator beam is Gaussian with a beam waist w_0 focused at the front facet, and is injected at the point $(x, z)=(x_{IN},0)$ on the BAL at an angle θ_0 with respect to the z-axis. The internal beam is allowed to diverge as it propagates through the cavity, and we can write the total output field $E_T(x,z)$ as:

$$E_T(x,z)=\sum_{i=1}^{N}E_i(x,z) \tag{1.1}$$

where N is the number of passes the injected beam makes through the laser, and $E_i(x,z)$ is the Gaussian beam emitted from the device after the ith pass (for i = 1,......., N).

Since the injected beam is refracted as it enters the broad area laser according to Snell's law, the ith Gaussian beam propagates as though it had originated from the point (x_{ai},z_{ai}) as shown in Figure 1.3, where:

$$x_{ai} = x_{in} + i \cdot \left(\frac{L'}{n} \sin\theta_0 - 2L\tan\theta_I \right) \qquad (1.2)$$

$$z_{ai} = -i \cdot \frac{L'}{n} \cos\theta \qquad (1.3)$$

$$L' = \frac{2L}{\cos\theta_I} \qquad (1.4)$$

$$\sin\theta_I = \frac{1}{n} \sin\theta_0 \qquad (1.5)$$

where L is the length of the broad area laser, L' is the actual distance traveled by the beam in one round trip, and θ_I is determined by Snell's Law. Phase distortion caused by the slight tilt of the beam is neglected.

The apparent phase propagation length inside the device is also different from that outside due to the internal index of refraction, so we must also determine an apparent origin of phase propagation (x_{pi}, z_{pi}) for the ith beam in the device. The coordinates for this origin are given as:

$$x_{pi} = x_{in} + i \cdot \left(L' n \sin\theta_0 - 2L\tan\theta_I \right) \qquad (1.6)$$

$$z_{pi} = -i \cdot L' n \cos\theta_0 \qquad (1.7)$$

To arrive at the total output field $E_T(x,z)$ for $z > 0$ (outside of the device), we determine the contribution from each Gaussian beam pass and then sum over all of the passes. The point (x,z) outside of the device must be transformed into the coordinate system aligned with the beam inside of the device. Using rotation matrices and the external angle of emission $-\theta_0$, the transformed apparent origin of the amplitude of the ith beam $(\hat{x}_{ai,}\hat{z}_{ai})$is given as:

$$\begin{bmatrix} \hat{x}_{ai} \\ \hat{z}_{ai} \end{bmatrix} = \begin{bmatrix} \cos\theta_0 & \sin\theta_0 \\ -\sin\theta_0 & \cos\theta_0 \end{bmatrix} \cdot \begin{bmatrix} x - x_{ai} \\ z - z_{ai} \end{bmatrix} \tag{1.8}$$

and similarly, the transformed apparent origin of the phase of the ith beam $(\hat{x}_{pi,}\hat{z}_{pi})$ is given as:

$$\begin{bmatrix} \hat{x}_{pi} \\ \hat{z}_{pi} \end{bmatrix} = \begin{bmatrix} \cos\theta_0 & \sin\theta_0 \\ -\sin\theta_0 & \cos\theta_0 \end{bmatrix} \cdot \begin{bmatrix} x - x_{pi} \\ z - z_{pi} \end{bmatrix} \tag{1.9}$$

We now have determined the apparent coordinates of the amplitude and phase origin from the ith Gaussian beam emitted from the device, as observed from outside the device. Using these points of origin, the electric field for the ith Gaussian beam at the point (x,z) is given by:

$$E_i(x,z) = E_0\sqrt{\frac{w_0}{w}} \cdot \exp\left\{-j\left[k_0\hat{z}_{pi} - \eta\right] - (\hat{x}_{ai})^2\left(\frac{1}{w^2} + \frac{jk_0}{2R}\right)\right\} \tag{1.10}$$

where the Gaussian beam parameters are defined as:

$$w^2 = w_0^2\left[1 + \left(\frac{\lambda\hat{z}_{ai}}{\pi w_0^2}\right)^2\right] \tag{1.11}$$

$$\eta = \frac{1}{2}\tan^{-1}\left(\frac{\lambda \hat{z}_{ai}}{\pi w_0^2}\right) \qquad (1.12)$$

$$R = \hat{z}_{ai}\left[1 + \left(\frac{\pi w_0^2}{\lambda \hat{z}_{ai}}\right)^2\right] \qquad (1.13)$$

$$k_0 = \frac{2\pi}{\lambda} \qquad (1.14)$$

and where w_0 is the half-width of the beamwaist as measured at the e^{-2} power points.

The near-field distribution (at the front facet z=0) is given by:

$$|E_T(x,0)|^2 \qquad (1.15)$$

and the far-field intensity distribution as a function of θ is given by:

$$|E_T(r\sin\theta, r\cos\theta)|^2 \qquad (1.16)$$

for very large distance r.

This model was incorporated into a Fortran computer program which was written and run on a Compaq 386 PC-clone computer. The basic parameters of the device which were used in the program are given in Table II. The resolution of the points on the x- and z-axes was 0.1 µm. All calculations in the far-field were determined using a radius value r of 95,000 µm (95 mm.). The number of passes through the device N was calculated using:

$$N = \frac{\left(w_{BAL} - x_{in}\right)}{2L\tan\theta_I} \tag{1.17}$$

where w_{BAL} is the active stripe width of the broad area laser. For the typical injection angle of 5°, the number of passes through the device was calculated to be 12.

The calculated near-field and far-field patterns for a 5 μm beamwaist injected at 5° are shown in Figures 1.4 and 1.5. Qualitatively, the far-field pattern consists of an interference pattern within a Gaussian envelope. The interference pattern is formed by all of the coherent passes emitted from the device, and the spacing of the fringes is a function of both the injected angle θ_0 and the injected wavelength λ. The angular width of the Gaussian envelope corresponds to the far-field diffraction pattern width expected for the injected Gaussian beam with full beamwaist $2w_0$. By examining the calculated far-fields versus spot size, it is observed that the locking bandwidth of the single lobe increases as the injected Gaussian beamwaist $2w_0$ decreases, but the fraction of total power coupled into the single lobe increases with increasing beamwaist $2w_0$. This predicted behavior agrees with the experimental behavior reported previously [8]. The model and experimental observations both agree that the optimum single lobe coupling efficiency and locking bandwidth are achieved when the injected Gaussian beamwaist $2w_0$ is half the width of the broad area laser aperture w_{BAL}. This result will be used in Section 2.5 to design the optimal optical system for our MOPA configuration.

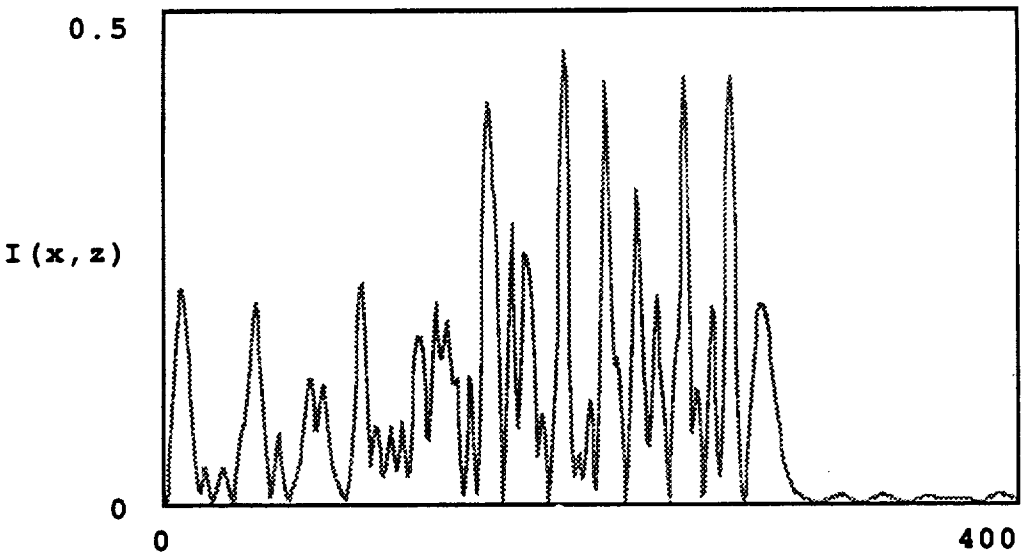

Figure 1.4: Calculated near-field pattern of injected broad area laser by Gaussian beam with beamwaist of 5 um, injected at 5° off of the facet normal.

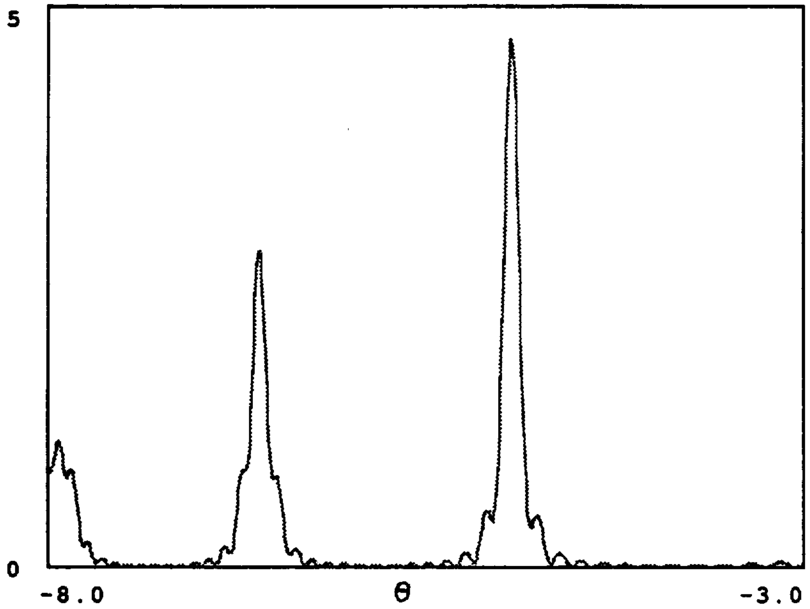

Figure 1.5: Calculated far-field pattern of injected broad area laser by Gaussian beam with beamwaist of 5 um, injected at 5° off of the facet normal.

1.3 Gain Model of Reflective Fabry-Perot Amplifier

As stated previously, the behavior of the injected broad area semiconductor optical amplifier is best described using a two-dimensional model which incorporates transverse propagation of the injected beam through the device and also spatially- and intensity-dependent gain and index properties [24,25]. It was also noted that the complexities of these models do not offer closed form solutions or yield intuitive or qualitative descriptions of the behavior of the device. It is our desire to simply investigate the two-dimensional properties which yield diffraction-limited beams from these devices while being able to make some qualitative predictions about the dynamic behavior of these devices.

In Section 1.2, we presented a simple model which describes the two-dimensional Gaussian beam propagation through the device, but ignores the spatially-dependent gain and index behavior by assuming that the gain is saturated to a round-trip value of unity [8]. We now present a qualitative discussion on the gain mechanisms present in the broad area amplifier, by making some one-dimensional assumptions about the behavior of these properties. We will later compare our experimental observations with the simple assumptions and qualitative predictions that we have made.

In the previous section, it was determined both theoretically and experimentally that the optimum injected beamwaist $2w_0$ is half the width of the broad area device aperture. For an injection angle of 5°, the internal Gaussian beam is displaced only a few microns between each pass, which implies a large amount of overlap between passes. Using this observation, we assume that to first order the transverse variations in gain may be neglected. This leads to a one-dimensional picture of the amplifier as a reflective Fabry-Perot cavity loaded with gain, as shown in Figure 1.6. The field reflectivities of the front and rear facets are given as *r1* and *r2*, respectively, and the G_S is the single-pass power gain. Disregarding phase shifts due to gain effects (for the present), the phase delay of each round-trip through the cavity δ is given by:

$$\delta = \frac{4\pi nL\cos\theta}{\lambda} \tag{1.18}$$

where L is the length of the device, θ is the injected angle, n is the index of refraction in the device, and λ is the free-space injected wavelength.

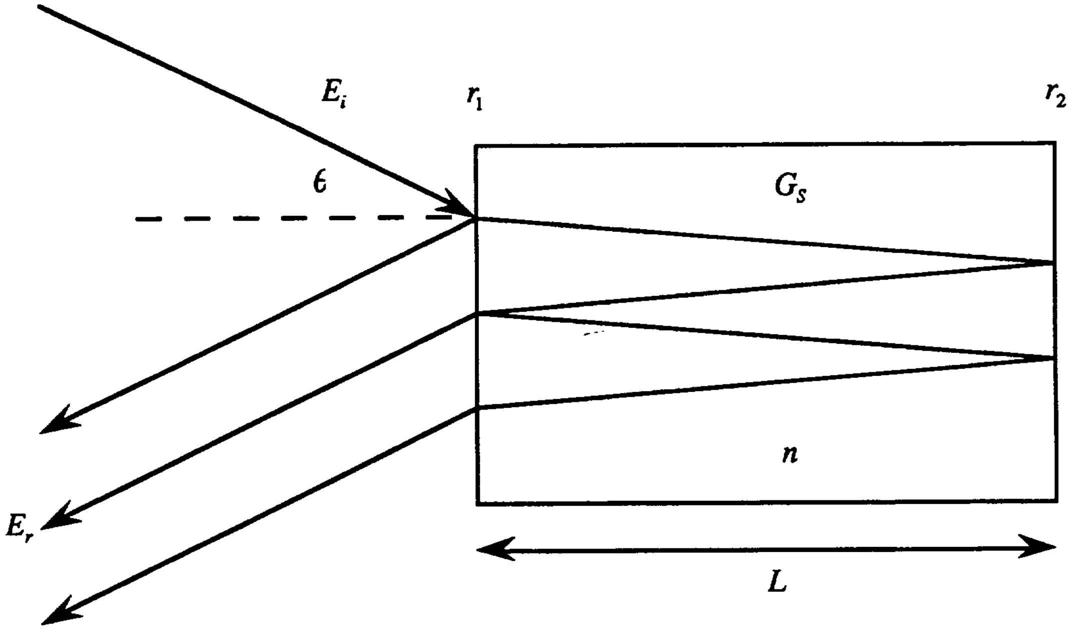

Figure 1.6: One-dimensional reflective Fabry-Perot amplifier model for broad area laser.

Summing the amplitudes of each of the reflected passes (and using a formula for the sum of an infinite geometric series) yields:

$$E_r = \left[\frac{r_1 - r_2 G_s e^{i\delta}}{1 - r_1 r_2 G_s e^{i\delta}} \right] E_i \tag{1.19}$$

and the total gain of the reflective amplifier G_c is found to be:

$$G_c \equiv \frac{I_r}{I_i} = \frac{R_1 + R_2 G_s^2 - 2\sqrt{R_1 R_2} G_s \cos\delta}{\left(1 - \sqrt{R_1 R_2} G_s\right)^2 + 4\sin^2\left(\frac{\delta}{2}\right)\sqrt{R_1 R_2} G_s} \tag{1.20}$$

where the power reflectivities R_1 and R_2 are defined as the squares of the field reflectivities r_1 and r_2, respectively. This result demonstrates that the gain will vary as a function of injected wavelength λ due to the Fabry-Perot resonances from the residual facet reflectivities. This effect is known as gain ripple. The value of total gain G_c approaches infinity asymptotically at the point where the single-pass power gain G_s equals the losses of the cavity. This value is simply expressed as:

$$G_s = \frac{1}{\sqrt{R_1 R_2}} \tag{1.21}$$

At this point, the amplifier begins self-oscillation, and becomes a laser.

Further examination of Equation (1.20) reveals that the single-pass gain G_s can be experimentally determined by measuring the ratio v of the reflected beam intensities resonant and anti-resonant with the cavity, using the expression:

$$\nu \equiv \frac{I_{\max}}{I_{\min}} = \frac{\left(\sqrt{R_1}-\sqrt{R_2}G_s\right)^2}{\left(1-\sqrt{R_1R_2}G_s\right)^2}\cdot\frac{\left(1+\sqrt{R_1R_2}G_s\right)^2}{\left(\sqrt{R_1}+\sqrt{R_2}G_s\right)^2} \qquad (1.22)$$

Examination of (1.20) also reveals that the point where the total gain G_C is 3 dB down from its peak value can be computed as a function of δ (which is a function of injected wavelength λ). This in turn will yield the 3 dB-frequency bandwidth of the gain peak, Δf_{3dB} , where the relation between frequency deviation and wavelength deviation is given by:

$$\Delta f_{3dB} = \frac{c}{\lambda^2}\Delta\lambda_{3dB} \qquad (1.23)$$

By numerically solving (1.20) in conjuntion with (1.23), we find the relationship between the 3 dB-frequency bandwidth and the total gain of the amplifier, as shown in Figure 1.7.

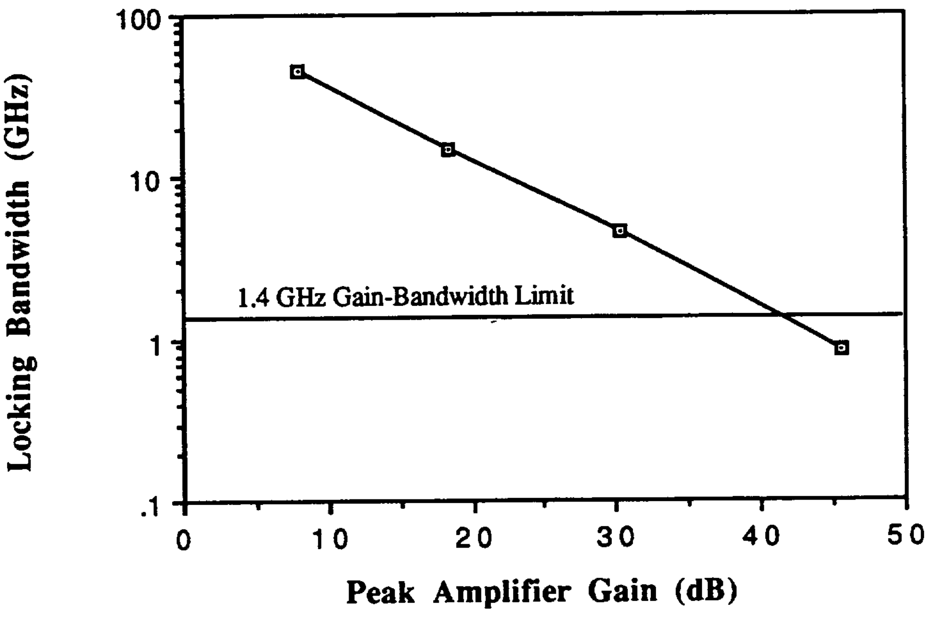

Figure 1.7: Calculated locking bandwidth versus peak amplifier gain (from parameters given in Table II).

The value of the gain-bandwidth product is calculated using only the cavity parameters, as given in [30]:

$$g_0\Delta\omega_{3dB} = \frac{(1-r_1)(1-r_2)}{\sqrt{r_1 r_2}} \cdot \frac{\Delta\omega_{FP}}{\pi} \qquad (1.24)$$

where $\Delta\omega_{FP}$ is the frequency spacing of the Fabry-Perot resonances, in radians. The validity of these calculations will be determined by examining the experimental observations to be presented in Section 3.

The gain properties of the amplifier can also be analytically-derived. We will use the single-mode rate equations to express the photon and carrier densities in the cavity, as follows [31]:

$$\frac{dS}{dt} = -\frac{S}{\tau_p} + \frac{A_g \Gamma N_e c}{n_g V_0} + A_g \Gamma (N_e - N_0)\frac{c}{n_g} S + S_{in} \qquad (1.25)$$

$$\frac{dN_e}{dt} = \frac{I_{th}}{eV_0}\frac{I}{I_{th}} - \frac{N_e}{\tau_c} - A_g (N_e - N_0)\frac{c}{n_g} S \qquad (1.26)$$

The parameters in the equation have been defined in Table II. The amplified spontaneous emission terms have been ignored (which would have required the use of multimode rate equations), in order to simplify the expressions.

For no saturation of the gain, we can express the single-pass power gain as:

$$G_s = \exp\left[\left(g_0(N_e) - \alpha\right)L\right] \qquad (1.27)$$

where the unsaturated material gain coefficient per unit length g_0 is expressed as:

$$g_0(N_e) = A_g\Gamma(N_e - N_0) \tag{1.28}$$

If we represent the number of photons in the active region in terms of the optical intensity I, where I is given by:

$$I = h\upsilon\frac{c}{n_g}S \tag{1.29}$$

then we can discuss a saturated gain coefficient $g(N,I)$, which is defined for a homogeneously-broadened system as [31]:

$$g(N_e,I) = \frac{g_0(N_e)}{1+\frac{I}{I_S}} \tag{1.30}$$

where the saturation intensity I_S is defined in a semiconductor laser as [31]:

$$I_S = \frac{h\upsilon}{A_g\tau_c} \tag{1.31}$$

The expression for the single-pass output intensity from the amplifier is a non-linear differential equation which must be solved numerically. In addition, the presence of the gain in a resonant cavity further complicates the expression for the output intensity. We will not attempt to develop this expression at this time.

It was previously derived [31] that the saturation intensity can be related to the experimentally-measured saturation output intensity I_{3dB}, which is defined as the intensity at which the signal gain has fallen 3 dB from the unsaturated value G_0. The relation is such that:

$$I_S \approx \frac{I_{3dB}}{\ln 2} \qquad (1.32)$$

According to this expression, the saturation intensity I_S is larger that the CW saturation output intensity I_{3dB} by 1.6 dB. We can therefore use our experimentally-measured value for I_{3dB} to estimate the CW saturation intensity of the amplifier, I_S.

1.4 Theoretical Effects of Modulation

Any theoretical treatment of the response of the amplifier to a time-varying or modulated input would need to examine the time-varying behavior of the carrier density and the photon density as a function of time, which is directly determined by the rate equations for the device as given in Equations (1.25) and (1.26). For pulse amplification, the rate equations can be used to determine the gain of the amplifier as a function of time. If the pulsewidth of the input pulse is much shorter than the carrier lifetime τ_c, which is typically 1-2 nsec in AlGaAs semiconductors, then the carrier density N_e can be approximated to be constant over the time of the pulse, and the temporal gain of the amplifier can be derived in closed form [31,32]. However, if the injected pulsewidths are on the order of the carrier lifetime, then the rate equations must be solved numerically. For the scope of this work, we did not calculate the gain of the amplifier as a function of time. The large-signal square-wave modulated data to be presented in Section 3 is presented for only observation and discussion.

The small-signal modulation bandwidth of the BAL can also be determined by a rate equation analysis. For the case where the amplifier is biased below the self-oscillation threshold, the frequency bandwidth has been demonstrated to be on the order of several gigahertz (see Section 1.3). For the case where the amplifier is biased above the lasing threshold, the rate equation analysis can be directly applied as in [33], which yields an expression for the response of the photon density to a modulation signal at frequency f_m:

$$s(2\pi f_m) = \frac{-\left(\frac{i_{\mathrm{mod}}(2\pi f_m)}{eV_0}\right) B S_0 \Gamma}{(2\pi f_m)^2 - i(2\pi f_m)/\tau_c - i(2\pi f_m) B S_0 - B S_0/\tau_p} \qquad (1.33)$$

where B is defined as:

$$B = A_g \frac{c}{n_g} \qquad (1.34)$$

The calculated magnitude of the frequency response of the BAL biased at 1.4 I_{th} for a small-signal modulation current i_{mod} of 10 mA is shown in Figure 1.8. The calculated response is relatively flat until reaching the relaxation oscillation peak, which occurs at 700 MHz. It must be remembered that this calculation is based on the oscillation properties of the BAL, which we have assumed up to this point behaves like an amplifier under injection.

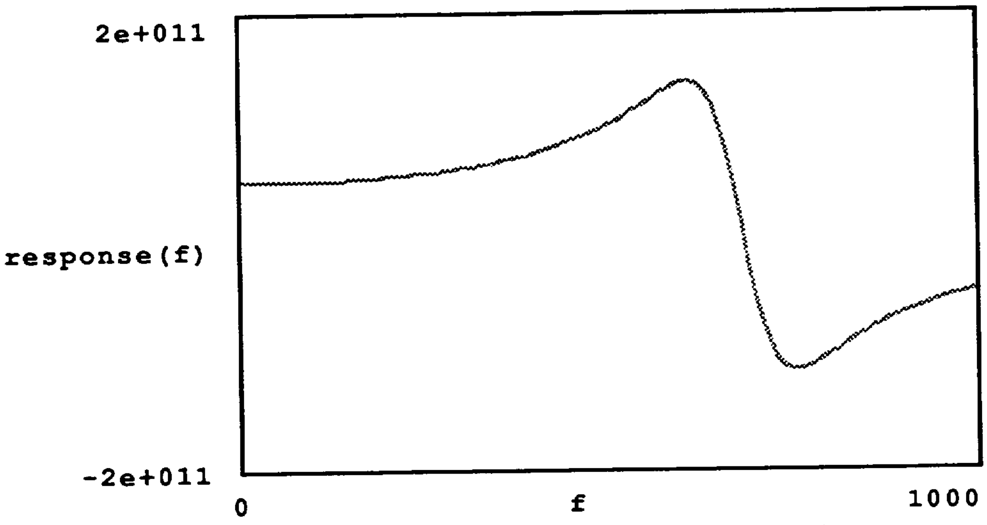

Figure 1.8: Calculated magnitude of the frequency response of BAL as an oscillator, for a small-signal modulation current of 10 mA. The bias of the BAL is 1.4 I_{th}.

It was our basic hypothesis at the outset of this work that the primary limiting factor to modulating the MOPA configuration would be the spurious FM modulation of the master oscillator, which is an artifact of the AM modulation of the laser. This FM modulation, or frequency chirp, would drive the injected frequency out of the locking bandwidth of the amplifier, and result in a drastically-reduced modulation response.

The magnitude of the frequency modulation is found to be a function of the frequency of the AM modulation [9]. Two mechanisms drive the frequency chirp: a thermally-induced temporal change in the index of refraction of the device at low frequencies, and a carrier-induced temporal index of refraction change at high frequencies.

The magnitude of the frequency chirp due to thermal effects can be expressed in general by [34]:

$$\Delta F(f_m) = \frac{\Delta F_{dc}}{\sqrt{1 + \frac{f_m}{f_c}}} \tag{1.35}$$

where ΔF_{dc} is the dc frequency tuning sensitivity of the laser, and f_c is a structurally-dependent cut-off frequency. Thermally-induced frequency chirp is generally non-existent at frequencies above 100 MHz [34].

A simple expression for the magnitude of the frequency chirp due to carrier effects is given as [35]:

$$\left|\Delta F(2\pi f_m)\right|_{f_m << f_R} = \left(\frac{i_{\mathrm{mod}}(2\pi f_m)}{eV_0}\right)\left(\frac{\alpha}{4\pi}\right)\frac{2\pi f_m \tau_p}{S_0} \tag{1.36}$$

where f_R is the relaxation oscillation frequency, and α is a parameter known as the linewidth enhancement factor, which relates the change in index to the change in carrier density. This equation shows that the carrier-induced frequency chirp is linear with modulation frequency, and dominates when the modulation frequency values are large. At a modulation frequency of 1 GHz, the frequency sensitivity calculated for the master oscillator is 150 MHz/mA using the parameters in Table II for 50 mW of average power.

In the next section, direct measurements of the frequency modulation of the master oscillator due to direct amplitude modulation will be presented. We will compare our results to the cursory theory presented here, to determine the validity of our measurements. We will then use the measured chirp values in Section 3 to compare with the measurements of the frequency response of the BAL.

Table I: Summary of Injection Locking-Amplifying Results to Date

Author/ Year	BAL Width [um]	BAL Pmax [mW]	Inj.BAL single lobe power [mW]	Lobe Width FWHM [deg]	Comments
Goldberg '85	100	100	105	0.5	First reported injection-locking of diode array
Hohimer '85	100	100	110	0.5	Second reported injection-locking of array
Goldberg '87	400	500	350	0.13	150 mW coupled into a 5-um core fiber
Abbas '88	100	100	80	0.5	Comprehensive amplifier model presented
Goldberg '88	160	1000	450	0.35	Saturation effects observed at 600 mW
Cornwell '89	100	500	240	0.5	Phasefront quality better than λ/30
Lucente '89	200	1000	310	0.5	Demonstrated 110 Mbps FSK modulation
Pang '90	400 (2)	1000	510	0.15	Two-stage injection-locking; AR-coated BALs
Goldberg '91	400	N/A	$2.6^{\dagger}$ W	0.12	0.5 μs pulse, 10% duty cycle. P_{in} = 365 mW
Goldberg '91	600	N/A	$12^{\dagger}$ W	0.08	0.5 ms pulse, 10% duty cycle. Pin = 500 mW
Livas '91	200	1000	120 mW	0.5	1 Gbps DPSK modulation

Table II: Device Parameters

<u>Broad Area Laser Parameters:</u>

Wavelength	λ	819	nm
Front facet reflectivity	R_1	0.02	
Rear facet reflectivity	R_2	0.95	
Laser length	L	500	µm
Quantum well width		200	Å
Waveguide height	d	0.8	µm
Active stripe width	w_{BAL}	400	µm
Volume of active region	V_0	3×10^{-10}	cm^3
Confinement factor	Γ	0.011	
group index of refraction	n_g	4.02	
Material loss constant	α_{loss}	2	cm^{-1}
Linewidth enhancement factor	α	3	
Photon density	S		
Transparency carrier density	N_o	1.44×10^{18}	cm^3
Instantaneous carrier density	N_e		
Threshold current	I_{th}	2.1	A
Differential gain	A_g	3.8×10^{-16}	cm^{-2}
Carrier lifetime	τ_c	1.5	nsec
Photon lifetime	τ_p		psec
Modulation frequency	f_m		MHz
Relaxation oscillation frequency	f_R		GHz

Section 2: Experimental Configuration

2.1 Introduction

In this section, the details of the experiment will be presented. The characteristics of the individual semiconductor laser devices will first be presented, which includes a rather detailed characterization of the modulation behavior of the master oscillator which includes the small-signal frequency response, frequency chirp, and square-pulse modulation behavior. The optical configuration of the MOPA will then be described, along with a description of the diagnostic system used to characterize the performance of the MOPA. The data and observations will be presented in the next section, where they can be discussed simultaneously with theory.

2.2 The Power Amplifier

The power amplifier used in this configuration is a custom-made gain-guided AlGaAs broad area laser (BAL), manufactured by Spectra Diode Laboratories. The amplifier is mounted in the open heat sink (or C-mount) package. The width of the active area is 400 μm, the length is 500 μm, and the height of the waveguide region is approximately 1 μm. The active layer consists of four quantum wells, and the confinement factor Γ is specified by the manufacturer to be 0.044. The rear facet has a high-reflectivity dielectric coating with an approximate power reflectivity R_h of 1.0. The front facet is anti-reflection (AR)-coated with a measured reflectivity R_a of 2.0 %. The amplifier chip is mounted active side down to allow cw as well as pulsed operation. The light vs. current curve at 25° C for the amplifier is shown in Figure 2.1; the lasing threshold occurs at 2.1 A, and the free-running output power at 2.9 A (1.4 I_{th}) is 530 mW. The measured external quantum efficiency is 0.511 W/A. The polarization ratio of the output at 500 mW was measured to be 26:1, in favor of the TE polarization.

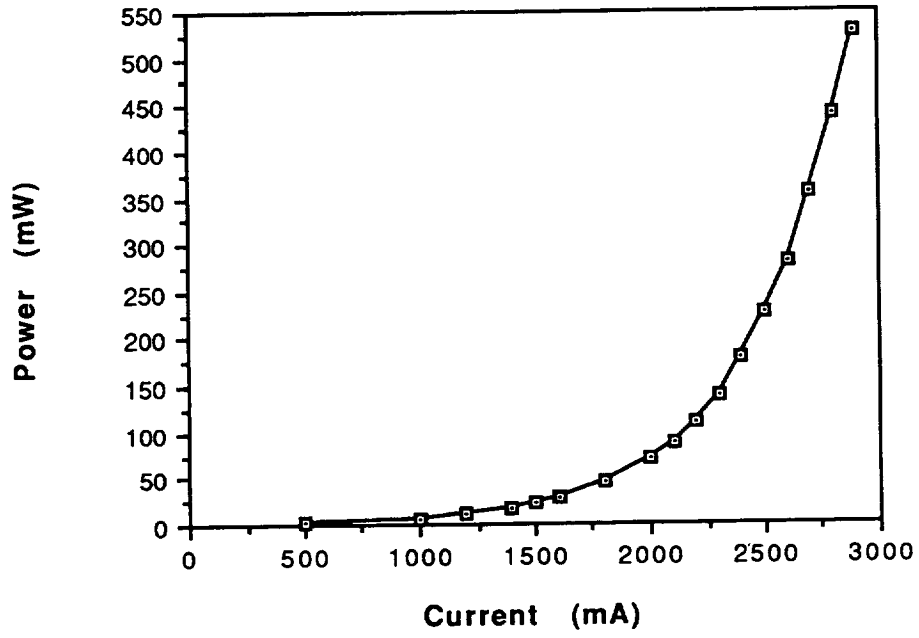

Figure 2.1 Power versus current curve for SDL broad area laser at 25.0° C.

The amplifier is dc biased by two SDL Model 800M current supplies, with a current stability of ± 1 mA. The temperature of the amplifier is held constant at 25.0° C using a control loop with a Peltier cooler, which is mounted to a water-cooled heat sink. At a dc bias of 3.0 A, the voltage across the amplifier is 2V, and the heat dissipated is 6W. The temperature of the amplifier is held stable to ± 0.1° C.

The output spectrum of the amplifier at 0.95 I_{th} (2.0 A) was measured to have a peak gain near 817 nm, with a half-maximum width of 7.8 nm. The free-running spectrum of the amplifier at 1.4 I_{th} ((2.9 A) demonstrated a peak gain centered at 820 nm, where the spectral bandwidth decreased to 1.0 nm. The peaks of the Fabry-Perot resonances (which result from the residual reflectivity of the front facet of the device) were observed to be spaced approximately 0.16 nm apart. The parameters of the broad area laser are summarized in Table II of Section 3.

2.3 The Master Oscillator

The master oscillator is a Spectra Diode Laboratories Model 5410 AlGaAs laser in the open heat-sink (or C-mount) package. This device is an index-guided, single quantum well- graded-index separate confinement heterostructure (SQW-GRINSCH) device which uses impurity-induced disordering to stabilize the output to a particular longitudinal mode over a 70 mW operating range. The light vs. current data for this device is shown in Figure 2.2. This specific device is capable of operating in the fundamental transverse spatial mode and a single longitudinal mode up to a CW output power of 200 mW. The polarization ratio of the output is measured to be better than 200:1 for the TM mode. The approximate wavelength of the laser output is 819 nm at 20.0° C, and can be tuned by changing the temperature or the dc bias of the laser. The temperature tuning rate was measured to be 0.07 nm/°C, while the current tuning rate was measured to be 3.5×10^{-3} nm/mA. The parameters of the master oscillator are summarized in Table II.

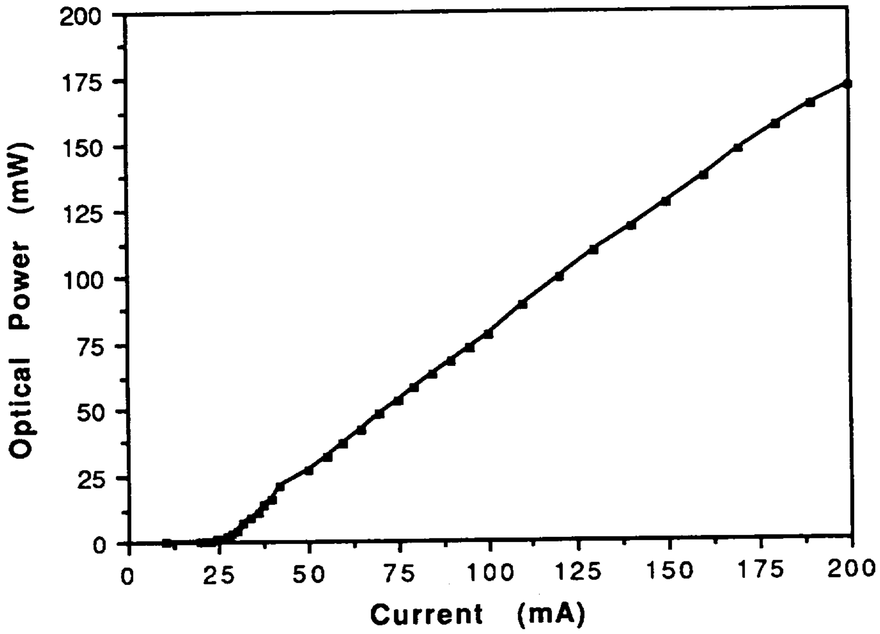

Figure 2.2: Power versus current curve for SDL 5410 master oscillator at 20.0° C.

2.4 Modulation of the Master Oscillator

2.4.1 The Modulation Electronics

The master oscillator is capable of both continuous wave (cw) and pulsed operation. The modulation electronics for the laser are shown in Figure 2.3. RF voltage signals from a modulation source are AC-coupled by a 1.0 μF capacitor across the laser, which is placed in series with a 50Ω 5W resistor on a microwave circuit board with 50Ω strip lines. A dc bias of up to 200 mA is supplied to the laser from two Keithley Model 220 current supplies via a 22 μH inductor. The current is stable to ±0.05 mA. The temperature of the laser is controlled to ±0.1° C using a Peltier cooler closed-loop control system.

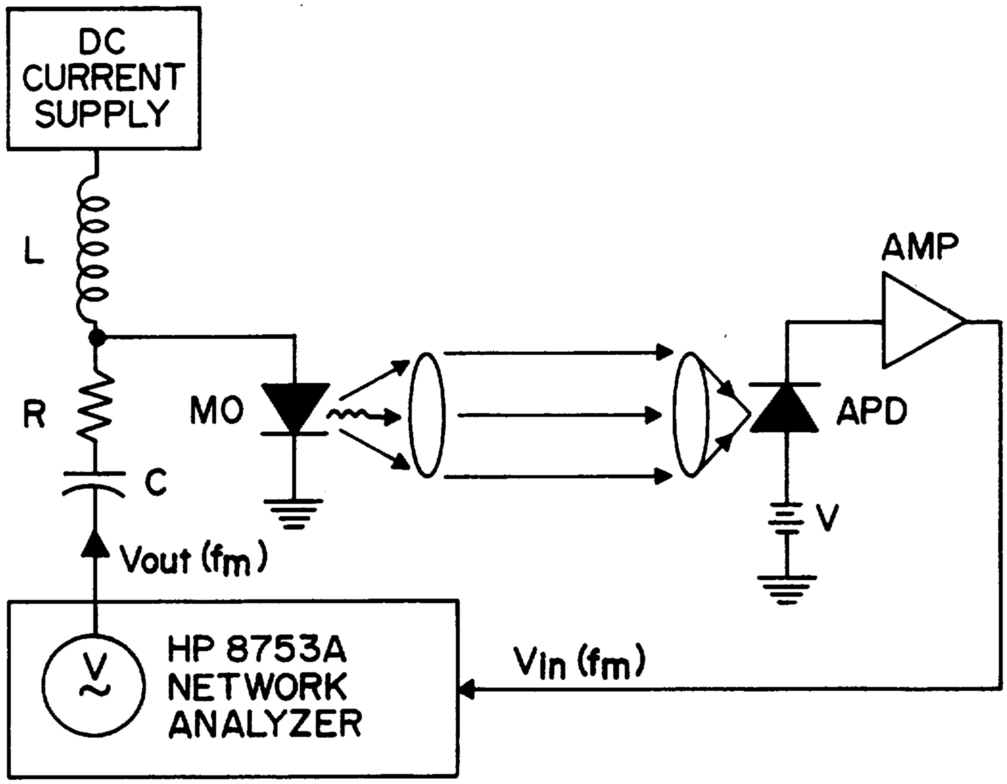

Figure 2.3 Master oscillator modulation electronics with optical detector and network analyzer.

The stability values of the temperature and current control imply a wavelength stability of ±0.007 nm for the laser.

2.4.2 Frequency Response of the Master Oscillator

Figure 2.3 also shows the configuration used to characterize the modulated behavior of the master oscillator, specifically the frequency response and the optical response to a square-wave input voltage.

The magnitude and phase of the frequency response of the master oscillator and its associated modulation electronics are characterized using a Hewlett-Packard Model 8753A Network Analyzer. The instrument generates a small sinusoidal voltage signal which sweeps in frequency from 300 kHz to 3 GHz. This signal is coupled into the master oscillator via the modulation electronics, resulting in a small intensity modulation superimposed on the cw intensity of the laser. The master oscillator beam is collimated and then focused down on an Opto-Electronics Model PD30 silicon avalanche photo-diode (APD) using an f/2.4 120 mm. focal length collecting lens. The APD output is amplified by a B&H Electronics Model DC3003 amplifier and returned to the input port of the network analyzer. The bandwidth of both the APD and the amplifier is specified to be from DC to 3 GHz.

For sinusoidal modulation frequency f_m, the total frequency response of the system $H(f_m)$ is defined as:

$$H(f_m) = |H(f_m)| e^{i\phi(f_m)} \tag{2.1}$$

which consists of both a magnitude and a phase $\phi(f_m)$. The magnitude of the frequency response $H(f_m)$ (in decibels) is determined by the relation:

$$|H(f_m)| = 10 \log \frac{P_{trans}(f_m)}{P_{in}(f_m)} \tag{2.2}$$

where the transmitted power $P_{trans}(f_m)$ and the incident power $P_{in}(f_m)$ are given by:

$$P_{trans}(f_m) = \frac{V_{S rms}^2}{R} \tag{2.3}$$

and:

$$P_{in}(f_m) = \frac{V_{APD\,rms}^{\;2}}{R} \tag{2.4}$$

where $V_{Source\ \ rms}$ and $V_{APD\ \ rms}$ are the rms voltages from the network analyzer and the APD/amplifier, respectively. The impedance of the system R is 50 ohms. The phase of the frequency response $\phi(f_m)$ is determined by comparing the absolute phase of the modulated master oscillator output at modulation frequency f_m with the output phase from a reference delay line with a known length that is internal to the network analyzer.

The temporal step response of the system can be calculated from the frequency response of the system. The step response $s(t)$ is determined by the convolution relation:

$$s(t) = h(t) \otimes u(t) \tag{2.5}$$

where $u(t)$ is the unit step impulse response, defined as:

$$u(t) = \int_{-\infty}^{t} \delta(t)dt \tag{2.6}$$

and $h(t)$ is the system temporal response, defined as:

$$h(t) = \int_{f_{start}}^{f_{stop}} H(f_m)e^{jf_m t}df_m \tag{2.7}$$

The network analyzer performs this transformation in discrete time, using the frequency response data, and generates a plot of the step response of the laser under test. The step response is indicative of the response of the laser to a low signal square-wave electrical pulse.

The magnitude of the frequency response for the master oscillator test system is shown in Figure 2.4. The master oscillator is biased at $I=2.9\ I_{th}$, which corresponds to an average power of 50 mW. The source power from the network analyzer is +10 dBm, which corresponds to an rms current variation of 10.2 mA into the laser and a sinusoidal optical intensity modulation of 10 mW. The frequency span of the test is from 300 kHz to 1 GHz, as the response of the modulation system is observed to roll off at 900 MHz. Data provided by the manufacturer demonstrates a frequency response for the laser which is flat to 3 GHz at 70 mW of average power, implying that the frequency response of the system is limited by the modulation electronics. The 1 dB ripple observed from 600 MHz to 1 Ghz indicates that the limited response is due to residual inductance and capacitance on the modulation board and bias lead wires to the laser. All subsequent frequency response data is collected over this limited frequency range from 300 kHz to 1 GHz.

The phase of the frequency response for the system is plotted in Figure 2.5, under the same conditions as the magnitude analysis. The value of the phase is shifted by 180° from the input phase, which is due to the inverting post-APD amplifier. The phase is relatively flat with frequency, except for a slight roll-off at higher frequencies.

The temporal step response of the system is plotted in Figure 2.6. The calculated rise time is approximately 1.5 nsec, and there is no appreciable ringing on the top of the pulse which would indicate a stimulation of relaxation oscillations. The apparent -3 nsec temporal displacement of the pulse is an artifact of the network analyzer, and is not indicative of any pulse turn-on delay or time shift.

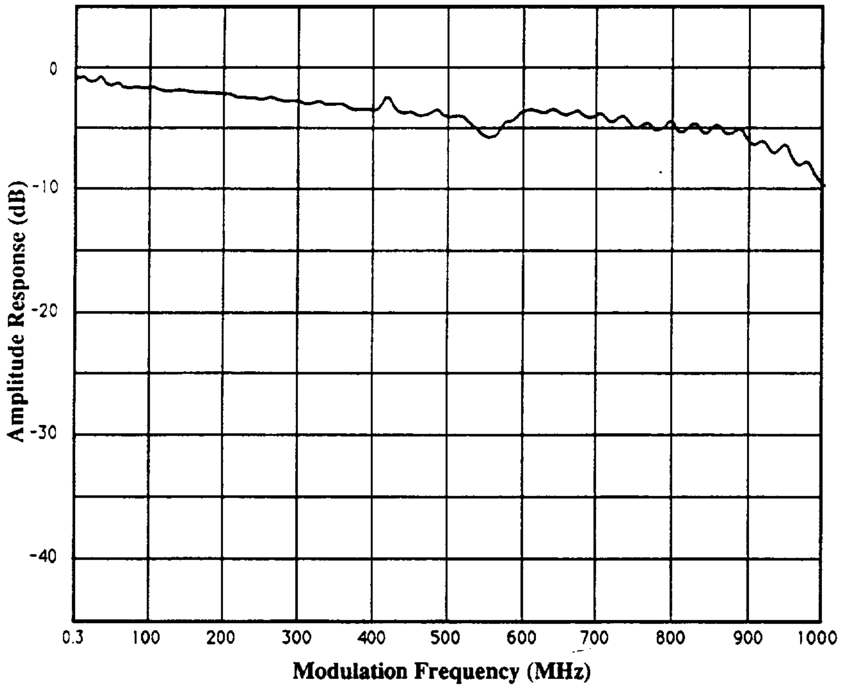

Figure 2.4: Magnitude of frequency response of master oscillator for P_{source} *= +10 dBm (10.2 mA rms).*

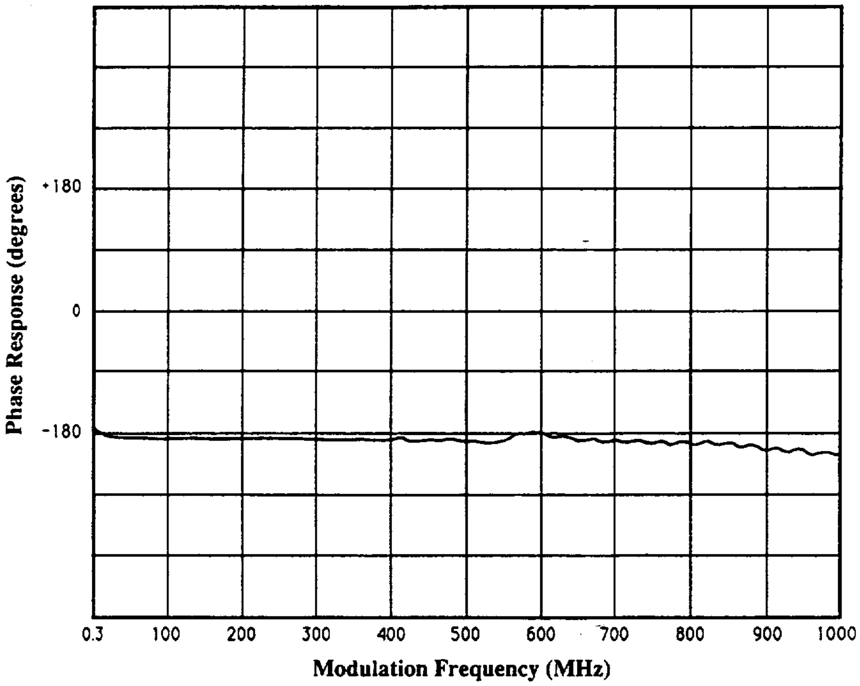

Figure 2.5: Phase of frequency response of master oscillator for P_{source} *= +10 dBm (10.2 mA rms).*

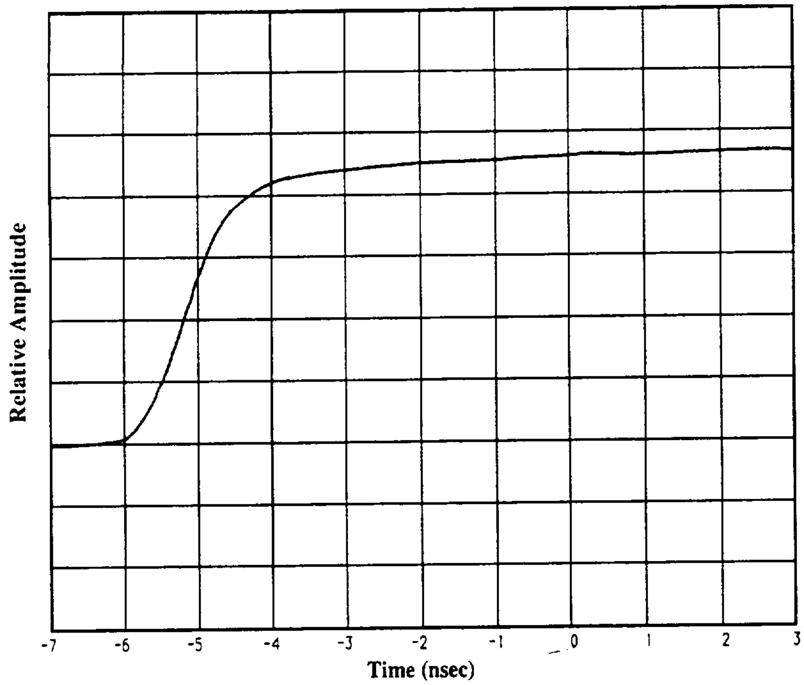

Figure 2.6: Step response of master oscillator computed from frequency response data at P_{source} *= +10 dBm (10.2 mA rms).*

The frequency and temporal response data of the master oscillator and associated modulation electronics will be used as reference data when later frequency and temporal response measurements of the MOPA configuration are presented.

2.4.3 Frequency Chirp of the Master Oscillator

Section 1.4 presented the well-documented observation that the intensity modulation (AM) of a semiconductor laser also produces a spurious frequency modulation (FM), which is commonly known as "frequency chirp". This frequency chirp is the result of temporal variations in the effective index of the waveguide region, which are caused by either thermal or carrier gradients in the device. The magnitude and mechanism of this chirp is a function of the applied modulation frequency. The effects of frequency chirp from the modulated master oscillator on the performance of the MOPA configuration were also discussed in Section 1.4. It was determined that a knowledge of the magnitude of the frequency chirp of the master oscillator is required to fully understand the implications of its effects on the MOPA performance. The frequency chirp of the master oscillator as a function of discrete sinusoidal modulation frequency was subsequently characterized for this research.

The optical field of the AM and spurious FM wave modulated at frequency f_m can be represented as [9]:

$$E = E_0\{1 + M\cos(2\pi f_m t)\}\cdot \exp[j\{2\pi f_0 t + \beta\sin(2\pi f_m t)\}] \tag{2.8}$$

$$f = f_0 + \Delta F\cos(2\pi f_m t) \tag{2.9}$$

where f is the instantaneous frequency and M is the amplitude modulation index. The phase modulation index β is defined in terms of the modulation frequency f_m and the maximum frequency deviation, or frequency chirp, ΔF, as follows:

$$\beta = \frac{\Delta F}{f_m} \tag{2.10}$$

The expression for the optical field (2.8) can be expanded into a sum of nth order Bessel functions, with the amplitudes of the carrier and first sidebands given as follows [9]:

Carrier:

$$J_0(\beta)E_0\exp\{j(2\pi f_0 t)\} \tag{2.11}$$

Upper first sideband:

$$\left[J_1(\beta)+\left(\frac{M}{2}\right)\{J_2(\beta)+J_0(\beta)\}\right]E_0\cdot\exp\{j2\pi(f_0+f_m)t\} \tag{2.12}$$

Lower first sideband:

$$\left[-J_1(\beta)+\left(\frac{M}{2}\right)\{J_2(\beta)+J_0(\beta)\}\right]E_0\cdot\exp\{j2\pi(f_0-f_m)t\} \tag{2.13}$$

It can be seen from these equations that if the AM and FM modulations are in phase, then the amplitude of the upper first sideband will be larger than that of the lower first sideband. If the AM and FM modulations become out-of-phase, the amplitude of the upper sideband will be smaller than that of the lower sideband. The amplitude modulation index M can be determined by comparing the ratio of the amplitudes of the two sidebands. In addition, the frequency modulation index β can be determined by the ratio of the average amplitude of the sidebands to the amplitude of the carrier. We will use this result in conjunction with a Fabry-Perot interferometer to measure the frequency chirp of the master oscillator.

The experimental configuration used to measure the frequency chirp is shown in Figure 2.7. The output of the master oscillator is collimated and passed through a Fabry-Perot interferometer onto a silicon p-i-n detector. The Fabry-Perot interferometer (FPI) consists of a resonant cavity formed by two high-reflectivity mirrors, one of

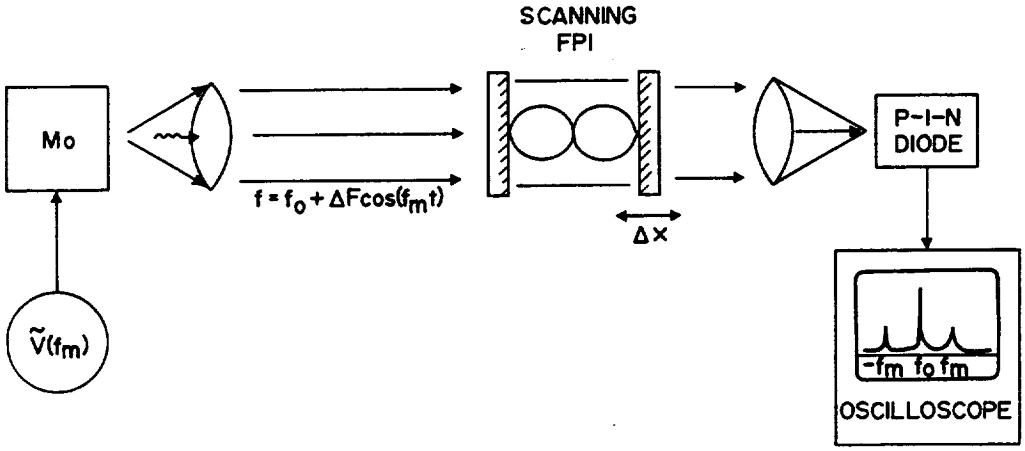

Figure 2.7: Experimental configuration for measuring frequency chirp of the master oscillator. The HP8753A network analyzer served as the sinusoidal modulation source.

which is linearly translated by a PZT so that the resonant peak transmission of the cavity is continuously swept in frequency. The 7.0 cm spacing of the cavity corresponds to a free spectral range of 2.1 GHz, and the measured frequency resolution was 80 MHz, which corresponds to a finesse of 26. The PZT-driven mirror was swept at 2 kHz.

The HP8753A Network Analyzer also served as the voltage source for the chirp measurements. The instrument was set to produce +10 dBm (ΔI=10.2 mA rms into 50 Ω) sinusoidal voltage signals at constant frequencies. The sinusoidal voltage was applied to the master oscillator, and the ensuing frequency spectrum was measured with the FPI. Figure 2.8 shows the frequency spectrum of the master oscillator at 500 MHz modulation. The spectrum consists of the carrier (at the laser oscillation frequency) and two sidebands centered at ± 500 MHz around the carrier frequency. The ratio of the intensity of the carrier to the average intensity of the two first sidebands is approximately given by equations (2.11) and (2.12) to be:

$$Ratio(\beta) = \frac{J_0(\beta)^2}{J_1(\beta)^2} \tag{2.14}$$

where the AM modulation index M is considered to be small. Assuming operation of the p-i-n diode in the linear regime as a square law detector, the voltage amplitudes of the carrier and of the two sidebands are measured and their ratio is determined. A computer program is used to numerically solve Equation (2.14) for the frequency modulation index value β which produces the equivalent ratio as measured with the FPI. This value of β is then

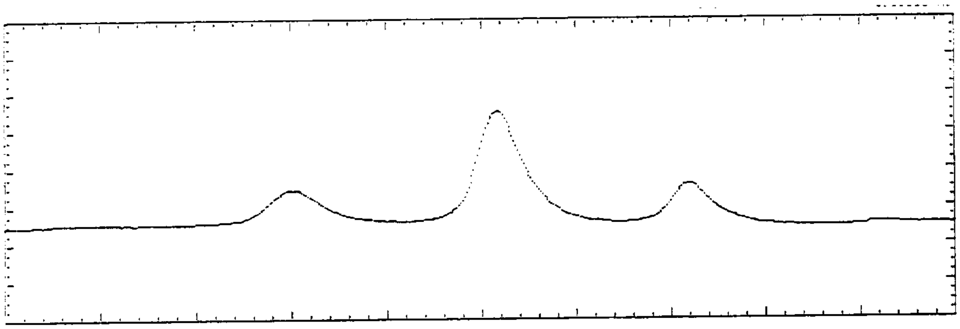

Figure 2.8: Optical spectrum of master oscillator with 500 MHz sinusoidal modulation, P_{source} = +10 dBm, as measured by a Fabry-Perot interferometer. The two sidebands are centered ± 500 MHz around the optical carrier frequency of the laser.

used in Equation (2.10) to determine the magnitude of the frequency chirp ΔF.

The frequency chirp of the master oscillator was characterized at cw operating powers of 50 mW and 170 mW, as a function of both modulation frequency f_m and modulation current ΔI. Figure 2.9 shows the measured frequency chirp of the MO as a function of modulation current for 500 MHz modulation at 170 mW cw operation. The chirp is observed to be linear with current, as is expected from theory and previous experimental observations [9].

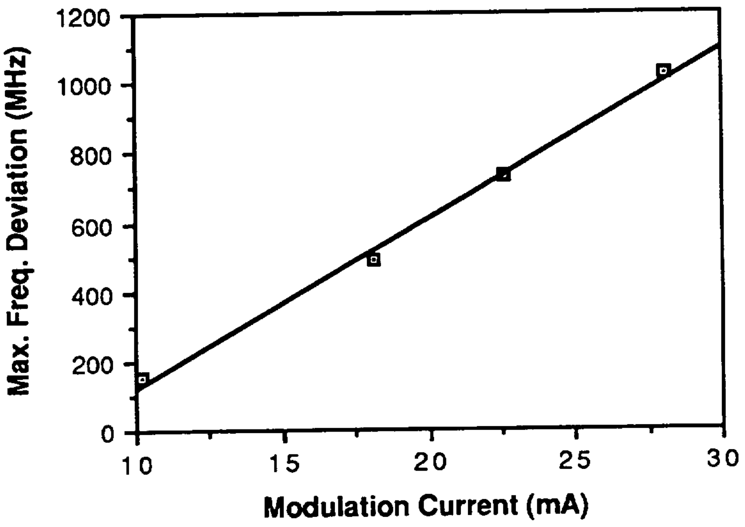

Figure 2.9: Frequency chirp of master oscillator vs. modulation current for 500 MHz sinusoidal modulation frequency at 170 mW cw operation.

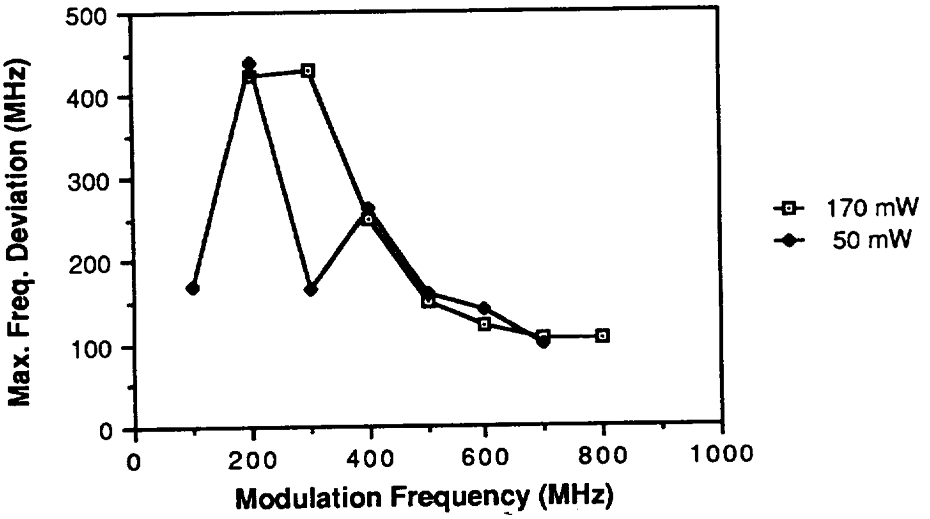

Figure 2.10: Frequency chirp of master oscillator vs. modulation frequency for cw intensities of 50 mW and 170 mW. The modulation current is constant at 10.2 mA rms (P_{source} = +10 dBm).

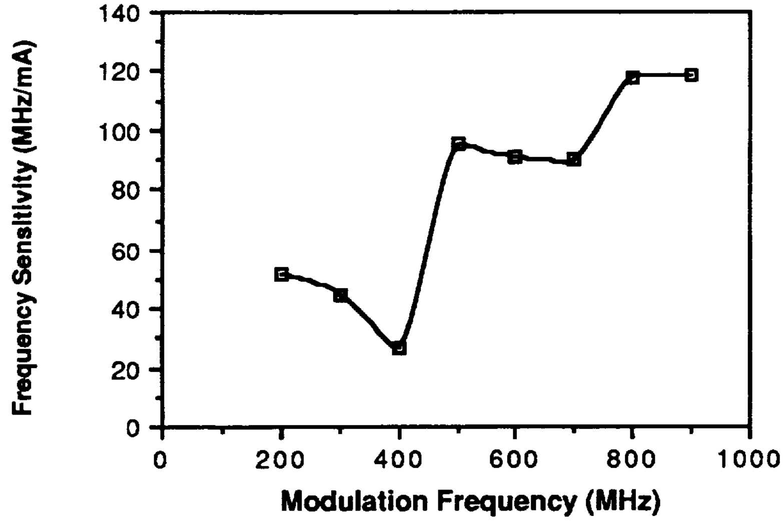

Figure 2.11: Frequency modulation sensitivity (in MHz/mA) as a function of modulation frequency for 50 mW average power.

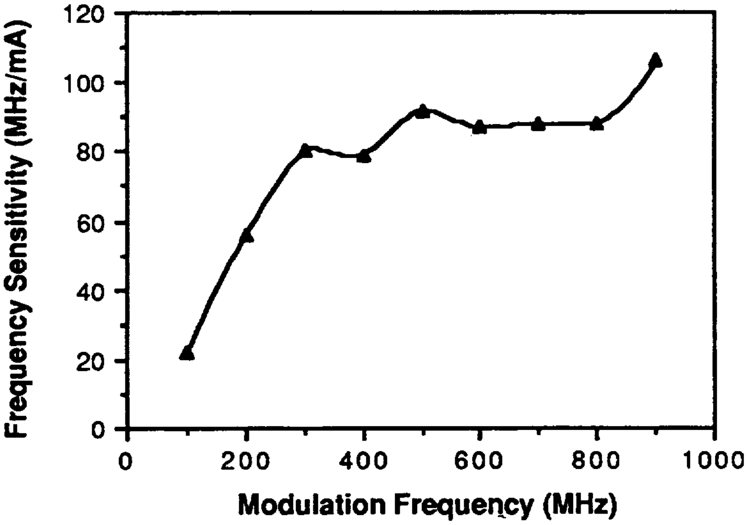

Figure 2.12: Frequency modulation sensitivity (in MHz/mA) as a function of modulation frequency for 170 mW average power.

The frequency chirp as a function of modulation frequency is shown for cw intensities of 50 mW and 170 mW in Figure 2.10, where the modulation power and current are constant at values of +10 dBm and 10.2 mA rms, respectively. The magnitude of the chirp for the two cw powers is approximately the same except at 300 MHz, which may be an errant data point. The amount of frequency chirp in general decreases with increasing modulation frequency. This result is basically an artifact of the frequency response of the modulation electronics, where the laser sees a smaller modulation current from the same modulation voltage at higher frequencies. The significance of the absolute frequency chirp data presented in Figure 2.10 will be realized when evaluating the frequency response measurements of the MOPA configuration, which will be discussed in Section 3.

The frequency modulation sensitivity of the master oscillator as a function of modulation frequency is shown in Figures 2.11 and 2.12 for 50 mW and 170 mW average powers, respectively. The FM sensitivity values are arrived at by finding the slope of a linear regression fit to the absolute frequency deviation versus current data for each modulation frequency f_m, where the current values have been adjusted by the magnitude of the frequency response of the modulation electronics at modulation frequency f_m (see Figure 2.4) as compared to the magnitude of the response at 100 MHz. This adjustment explains the absolute decrease in chirp with modulation frequency shown in Figure 2.10. The adjusted FM sensitivity curves of Figures 2.11 and 2.12 are also in closer agreement with previously-measured values and those predicted by theory, where the FM sensitivity is observed to generally increase with modulation frequency due to an increase in the carrier-induced index at frequencies above 100 MHz [9].

Neither the FM sensitivity nor the absolute frequency deviation of our master oscillator were measurable for frequencies below 100 MHz with our system, although we will later be considering frequency modulation data for frequencies down to 300 kHz. As a reference point for low modulation frequencies, the FM sensitivity of the MO was characterized at DC to be 1.5 GHz/mA. This value is a factor of 10 larger than the largest FM sensitivity measured at high modulation frequencies; therefore, we expect the frequency chirp to be very large for frequencies below 100 MHz.

The FM sensitivity of the master oscillator will be used in the next section to estimate the frequency chirp of the master oscillator when subjected to square wave intensity modulation, where the square wave is decomposed into its sinusoidal Fourier series components.

2.4.4 Square Wave Modulation of the Master Oscillator

One of the goals of this research program is to square-wave intensity modulate the master oscillator at frequencies of 10 MHz and 250 MHz, and subsequently observe the output of the MOPA configuration under these modulated conditions. This requires the behavior of the master oscillator to first be characterized under full square-wave intensity modulation. The relevant characteristics to be measured are the temporal and power properties of the pulses, the extinction ratio between pulses, and also the time-averaged optical spectrum of the master oscillator while under modulation.

The configuration for modulating and then characterizing the master oscillator is similar to the one shown in Figure 2.3. For this experiment however, the network analyzer is replaced by a Hewlett-Packard Model 8131A Pulse Generator, with a maximum square wave frequency of 500 MHz (50% duty cycle) and rise and fall times of 130 psec. The amplitude of the output voltage can be varied from 0-5 V_{pp}, which corresponds to a maximum of 100 mA of modulation current into 50 Ω. The voltage modulation signal is coupled to the master oscillator via the modulation electronics, where a dc bias is also applied. For square-wave modulation at 10 MHz and 250 MHz, the master oscillator is biased as shown in Figure 2.13. The dc current is set to produce the desired average power, which for full intensity modulation corresponds to 50 mW at 73 mA of bias. The 0 V to 5 V electrical pulses drive the current to the laser from 23 mA to 123 mA, which corresponds to an intensity modulation from threshold power of 3 mW to full power at 100 mW.

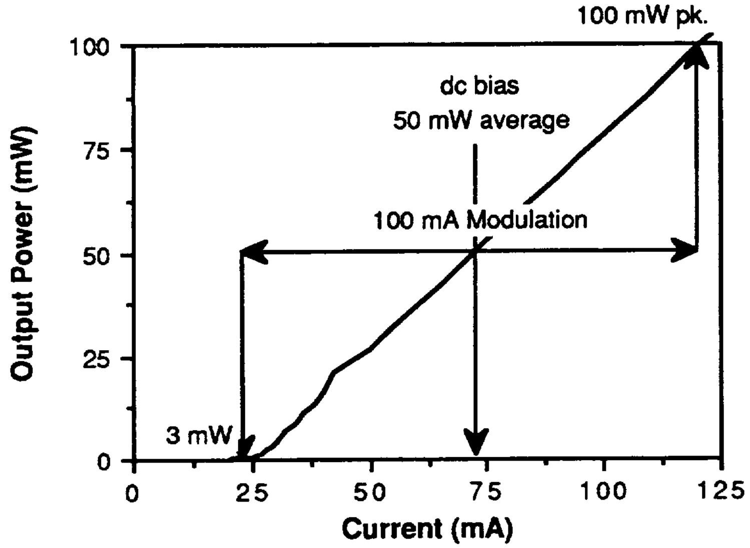

Figure 2.13: Power versus current curve for master oscillator demonstrating intensity variation for square-wave current modulation, 50% duty cycle.

The modulated output of the master oscillator is again collimated and then focused by a lens onto the Opto-electronics APD. The output of the APD and amplifier configuration (shown in Figure 2.3) is sent to a Tektronix Model 7104 oscilloscope with a 1 GHz bandwidth, and the temporal shape of the pulse is recorded with a Polaroid camera.

Prior to modulation, the frequency spectrum of the square waves from the HP 8131A Pulse Generator is analyzed using a Hewlett-Packard Model 8590A RF Spectrum Analyzer, which has a frequency bandwidth from 10 kHz to 1.5 GHz. The spectrum analyzer basically conducts a Fourier series analysis on the square waves, decomposing them into their sinusoidal component frequencies and their relative amplitudes. The frequency spectrum of the 10 MHz square wave pulse and the 250 MHz square wave pulses are shown in Figures 2.14 and 2.15, respectively. It must be noted that the frequency response of the modulation electronics is limited to 1 GHz (see Figure 2.4); the master oscillator will therefore only see the frequency components below 1 GHz.

The electrical pulses directly from the HP8131A pulse generator were also observed on the Tektronix oscilloscope before application to the laser. At 10 MHz, the voltage pulse was observed to be 49 nsec wide FWHM, with rise and fall times of approximately 600 psec. The amplitude of the pulse was 5.2 V. The pulse at 250 MHz was observed to have a FWHM width of 2.2 nsec, with rise and fall times of approximately 400 psec. The amplitude of the voltage modulation was 5.0 V.

The optical waveforms from the master oscillator as measured by the APD are shown in Figures 2.16 and 2.17. In Figure 2.16, the optical pulse at 10 MHz is observed to have a width of 50 nsec, with a 1.5 nsec rise time and a 2 nsec fall time. This rise time is in agreement with the rise time predicted by the calculated step response. The average power of the pulse is 50 mW. It is also observed that the peak of the pulse is approximately 100 mW, but varies over time by as much as 15 mW. This peak power variation is observed to be a function of the position of the APD in the far-field of the lens, which indicates that the beam from the master oscillator is steering during the pulses. This observation agrees with other research that will be published in the future [ref]. We will assume that this beamsteering will have a negligible effect on the performance of the MOPA. The extinction ratio of the pulse is observed to be approximately 20:1.

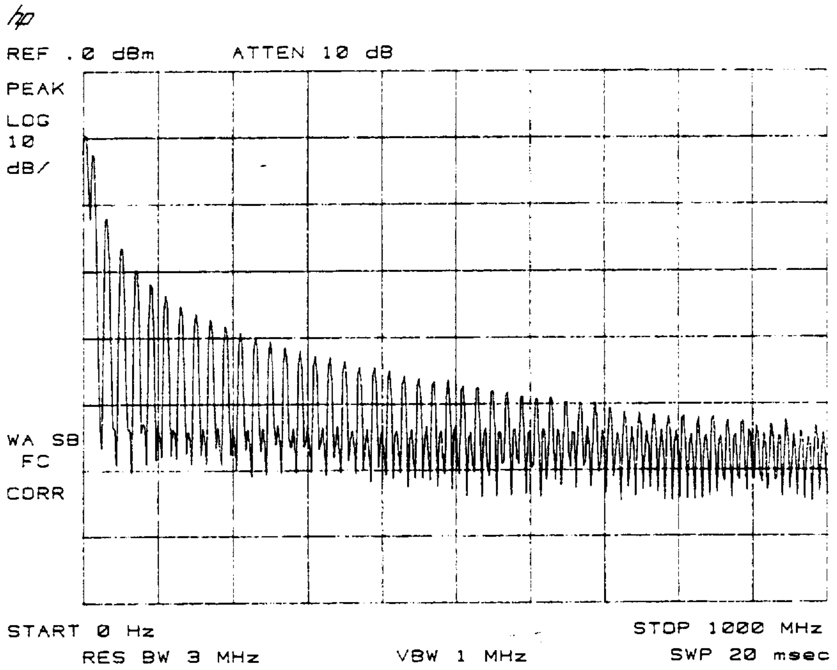

Figure 2.14: Frequency spectrum of square wave pulses at 10 MHz.

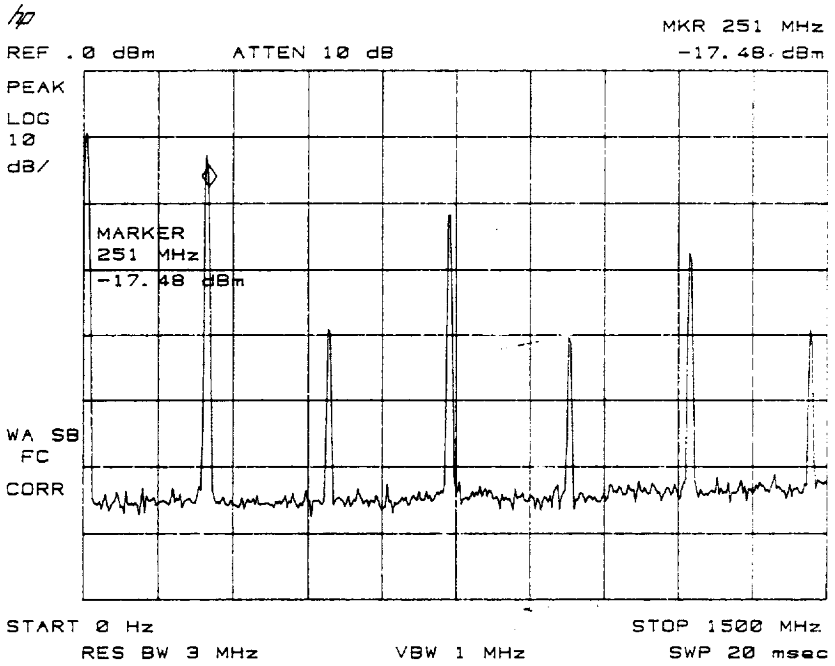

Figure 2.15: Frequency spectrum of square wave pulses at 250 MHz.

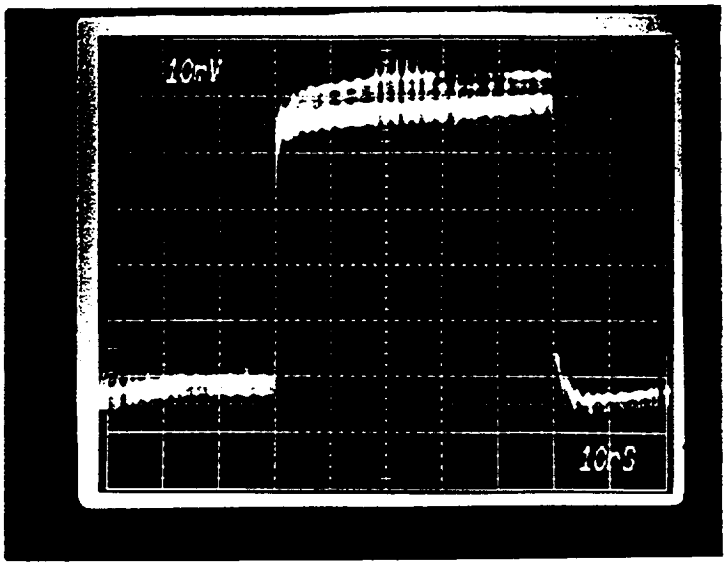

Figure 2.16: Optical pulse from modulation master oscillator at 10 MHz as measured by silicon APD.

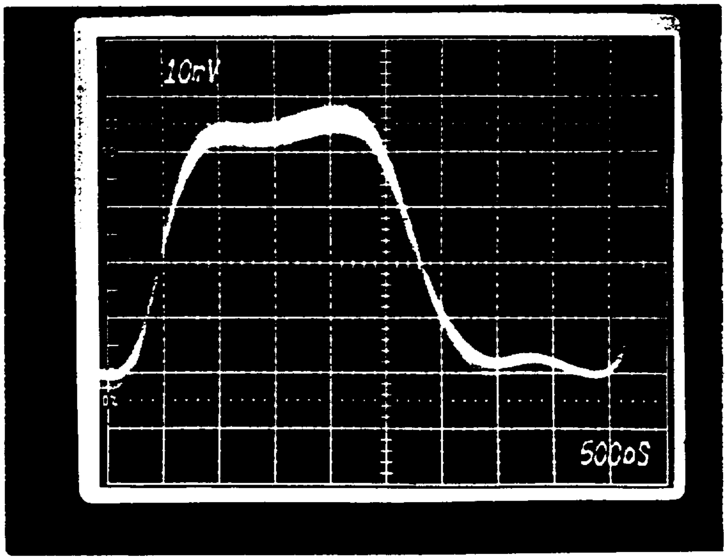

Figure 2.17: Optical pulse from modulated master oscillator at 250 MHz.

The optical pulse for 250 MHz modulation is shown in Figure 2.17. The measured pulsewidth FWHM is 2.3 nsec, with a rise time of 1 nsec and a fall time of 1.2 nsec. The average power of the pulse is again 50 mW, with the peak power remaining more stable in time at approximately 100 mW. The power in the "off" state has increased since the time interval between the pulses is on the order of the fall time of the pulses. This results in a reduction the extinction ratio to approximately 7:1.

The optical spectrum of the master oscillator was observed using a Candela Model LS-1 computer-controlled diffraction-grating spectrometer with a resolution of 0.01 nm. The master oscillator spectrum under modulation was observed to be single longitudinal mode at both 10 MHz and 250 MHz. This results in part from the DBR-type structure of the master oscillator, which acts to reinforce the gain of only a single longitudinal mode. This result is also due in part to the modulation conditions; as the laser is never driven below threshold current, it does not experience relaxation oscillations and other effects which can distribute gain to many longitudinal modes.

The optical spectrum was observed in greater detail using the Fabry-Perot interferometer. The spacing of the FPI mirrors was reduced to less than 1 mm., which corresponded to a measured free spectral range of 10 GHz. The time-averaged optical frequency spectrum for 250 MHz modulation is shown in Figure 2.18. The carrier is the peak to the far right; the peak to the far left is the next order of the carrier on the FPI. Only one sideband is present, which is the result of the large AM modulation index M. The sideband is displaced 8.3 GHz from the carrier frequency modulation in the beam cannot easily be determined, as the observed sideband is located at 8 GHz, which corrsponds to a Bessel function of order 32 in Equation (2.13).

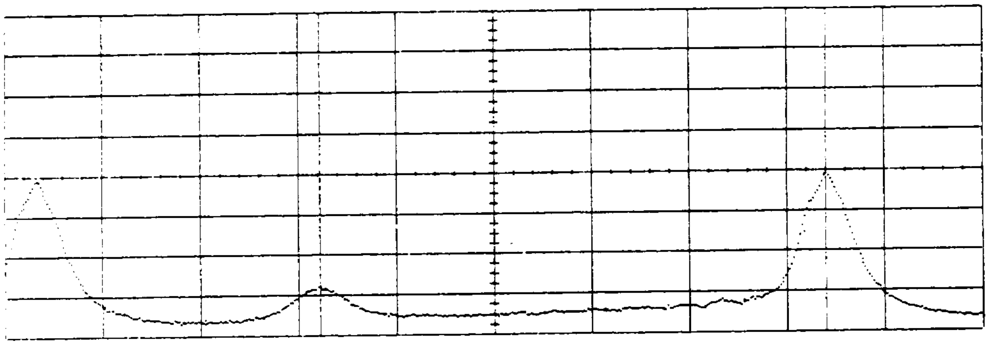

Figure 2.18: Optical spectrum of master oscillator at 250 MHz square wave intensity modulation as measured with a Fabry-Perot interferometer. The FSR is 10 GHz, and the frequency spacing between the carrier and sideband is 8.3 GHz.

2.5 Optical Configuration of the MOPA

The previous sections have presented the parameters and characteristics of the master oscillator and the power amplifier, the two constituent devices of the MOPA configuration. In this section, the detailed configuration of the MOPA will be presented along with the beam diagnostic system used to characterize the MOPA performance. The actual performance data and observations for the MOPA will be presented and discussed in Section 3.

In the MOPA scheme, the beam from the master oscillator must be efficiently coupled into the power amplifier by matching the polarization, frequency, and spatial position of the beams of the two devices. The optical system used to achieve this coupling is shown in Figure 2.19, and will be discussed in detail in the following paragraphs.

The output of the master oscillator is collected and collimated by a Liconix Model L-8012.0 mm. focal length diode laser collimating lens with a numerical aperture of 0.65. The collimated beam is then passed through two Optics For Research, Inc. Model NIR2-IO-5 optical isolators, which are each specified to produce -30 dB of isolation. These devices consist of a linear polarizer followed by a Faraday rotator and another linear polarizer oriented at 45° to the first polarizer. The initial linear polarization of the master oscillator is passed by the first polarizer, rotated 45° by the Faraday effect, and then passed through the second polarizer. Beams which enter from the opposite direction are polarized by the second polarizer and then rotated 45° by the Faraday rotator. This beam is now linearly polarized orthogonally to the first polarizer, and therefore does not

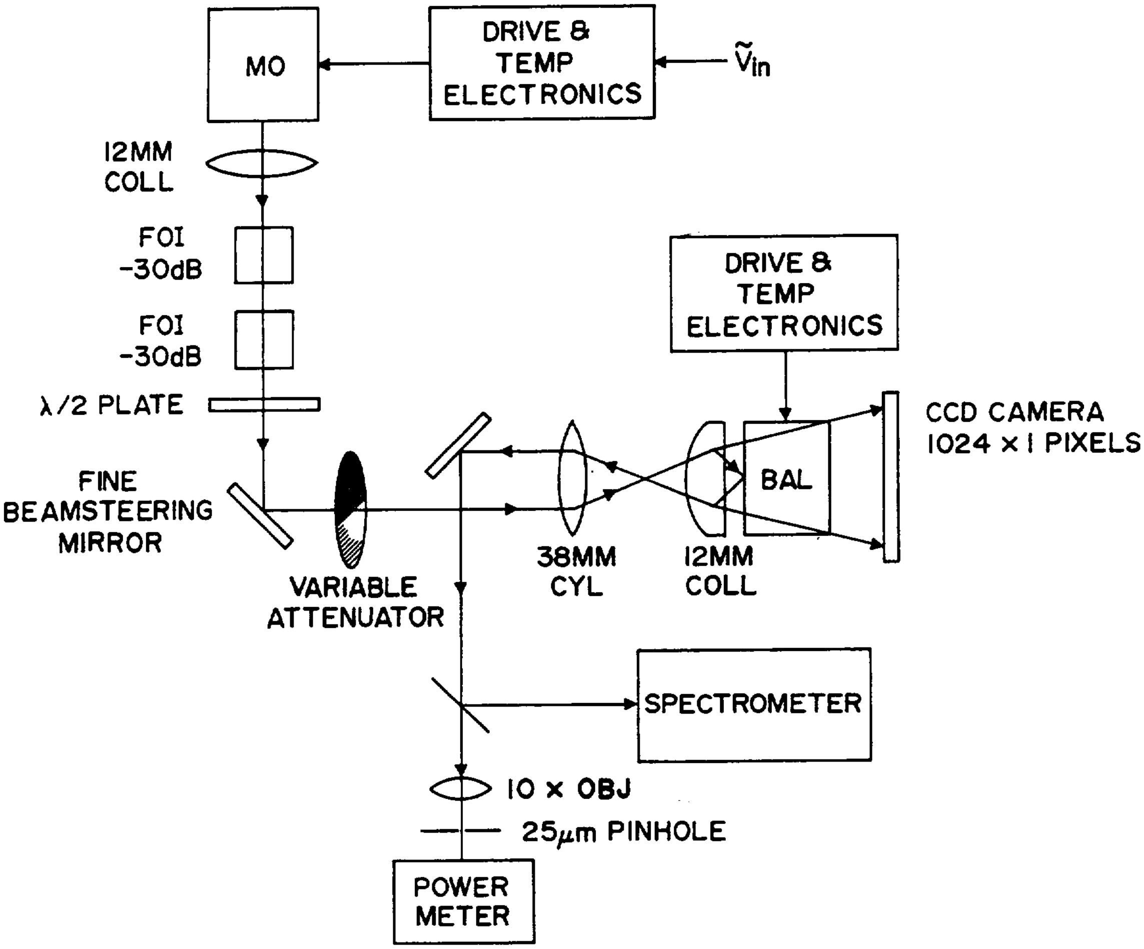

Figure 2.19: Optical configuration of the AlGaAs semiconductor laser MOPA scheme. Beam diagnostics for time-averaged measurements are also shown.

pass. The optical isolator insures that neither reflected light nor light from the amplifier feeds back into the master oscillator, a condition which can cause instabilities in the frequency and power of the master oscillator. A half-wave retarder plate (λ = 830 nm) is used following the second optical isolator to rotate the linearly-polarized beam from the isolator into the polarization plane of the amplifier. This insures that the polarization of the injected beam is matched to that of the amplifier to achieve maximum gain from the amplifier.

The beam is then incident on a turning mirror with a differential micrometer mount which is placed on a linear translation stage. The differential micrometers are capable of submicron motion, and together with the linear translation stage allow for the fine adjustment of the injection position and the injection angles on both the parallel and perpendicular axes to the amplifier active layer.

A variable neutral density filter is mounted on a wheel subsequent to the beamsteering mirror. This filter allows the injected power to be attenuated without changing the injected wavelength, which in turn allows the gain properties of the injected broad area laser to be characterized.

The beam from the mirror is directed through beamshaping optics which form a 200 μm x 5 μm focused spot at the front facet of the amplifier. The Fabry-Perot amplifier model of the BAL calculates this to be the optimum size of the injected beamwaist, which is half of the aperture width of the broad area laser. A computer program based on the Gaussian beam propagation model was written and used to design an optical system which would produce beamwaists of this size at the same focal plane for the two orthogonal transverse axes of the beam. The optimum lens system was determined to be a 38.0 mm. focal length cylindrical lens, placed 50 mm. before another Liconix Model L-80 12.0 mm. focal length spherical lens with a numerical aperture of 0.65. The collimating lens is placed 12 mm. in front of the amplifier to produce the proper beamwaists on the front facet.

The Fabry-Perot model also determines that the optimum single lobe far-field pattern results when the master oscillator beam is injected at one of the ends of the amplifier and at an angle of 4° to 5° to the amplifier facet normal. As mentioned previously, the injection angle can be varied using the mounted turning mirror with differential micrometers. The single lobe output is emitted -4° to -5° from the amplifier facet normal and is captured and re-collimated by the 12.0 mm. lens. The injected and output beams are therefore separated by approximately 2 mm., and a mirror with a knife edge can be used to "pick off" the entire amplified BAL output while leaving the injected beam undisturbed. The output beam is then sent off to a system of diagnostic equipment, which will be described in the following section.

The actual sizes of the beamwaists on both axes were measured using a linear CCD array camera, and were determined to be close to the 200 μm x 5 μm required beamwaists. Considering the 1 μm height of the amplifier waveguide and the transmission of the various optical elements, the overall coupling efficiency of the master oscillator beam to the amplifier is calculated to be 4%.

2.6 MOPA Beam Diagnostic System

2.6.1 CW or time-averaged measurements

The far-field radiation pattern of the broad area laser is continuously monitored using a 1024-element linear CCD array camera, as shown in Figure 2.19. The reflected output from the rear surface of the 12 mm. collimating lens is directed to the camera, which is placed such that the angular resolution of each pixel is 0.015°. Neutral density filters are placed between the amplifier and the camera to avoid saturating the CCD array.

The near-field pattern of the amplifier is also measured using a 1024-element linear CCD array camera. A Pellicle beamsplitter is placed before the 38.0 mm. cylindrical lens (see Figure 2.19) to reflect a fraction of the total amplifier output through a cylindrical lens, which produces a magnified image of the near-field of the broad area laser on the CCD array. When a screen is placed in front of the CCD array, the visible image can be used to align the injection beam with the broad area laser.

The optical spectrum of the amplifier output beam is measured by the Candela Model LS-1 spectrometer, which is also used to monitor the master oscillator wavelength to insure the stability and tunability of the single longitudinal mode output. An Ando Corporation Model AQ-1425 Optical Spectrum Analyzer with a resolution of 0.1 nm is also used, which has a logarithmic display to quantify the amplitude of the lower spectral modes as compared to the primary mode.

The time-averaged amplified power output is measured using a silicon photodiode power meter which is placed behind a spatial filter, allowing the amount of diffraction-limited power to be measured (see Figure 2.19). The spatial filter consists of a Newport Model 10X microscope objective and a 25 μm diameter pinhole. The diffraction-limited spot size of the microscope objective is calculated to be 23 μm using the manufacturer's data, which implies that only a near-diffraction-limited beam will be transmitted.

2.6.2 Modulated or time-varying measurements

The characterization of the modulated performance of the MOPA is very similar to that performed in the characterization of the master oscillator. Specifically, the frequency response and square-wave intensity modulation behavior are the primary measurements. In addition, aspects such as locking bandwidth and diffraction limited power under modulation are also characterized; the methods and results of these measurements will be discussed in Section 3.

The experimental configuration for the characterization of the frequency response is shown in Figure 2.20. The modulation electronics and frequency response measurement scheme are the same as those shown in Figure 2.3; the major difference in this configuration is the optical system used in front of the APD to measure the temporal behavior. The 10X microscope objective has been replaced by an f/2.5 Melles-Griot diode laser receiver lens with a 120 mm focal length, which produces a diffraction-limited spot of 30 μm according to the manufacturer's data. The 25 μm pinhole is again used to spatially filter the beam, but sampling only the most central portion of the diffraction-limited lobe from the MOPA.

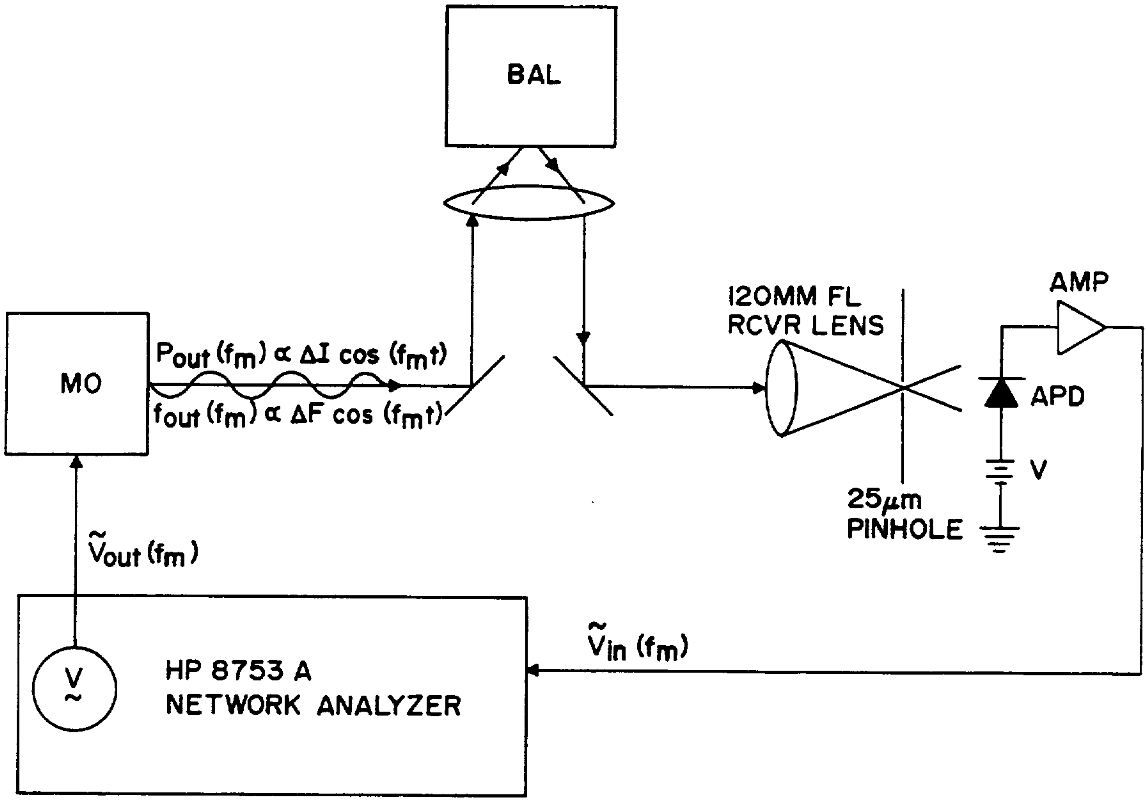

Figure 2.20 Experimental configuration for characterization of modulated MOPA performance; namely, frequency response and square wave pulse response.

In addition to the optics, the obvious difference is the testing scheme. In this scenario, the small-signal AM modulation is applied only to the master oscillator, which results in a well-characterized intensity- and frequency-modulation, as presented in Section 2.4. The AM/FM modulated output of the master oscillator is then injected into the amplifier, which responds in some way to the modulated input field. The modulated output of the amplifier is subsequently measured and fed back into the network analyzer via the APD, and the corresponding AM/FM frequency response is characterized. The results of that characterization will be presented in Section 3.

In addition to the measurement of the frequency response, the experimental configuration of Figure 2.20 was also used to characterize the square-wave modulation behavior of the MOPA. Again, the AM/FM modulation is applied to the master oscillator beam, which is injected into the amplifier, and again the ensuing amplifier output is characterized. The square wave modulation of the master oscillator is performed as described in Section 2.4, using the HP8131A Pulse Generator. The temporal properties of the optical pulse from the amplifier is monitored with an APD and an oscilloscope. The relevant properties to be measured are the pulse width, rise and fall times, average and peak powers, and the extinction ratio. The results of these measurements will be presented in the next section.

Section 3: Data and Discussion

3.1 Introduction

In this section, the results of the MOPA experiments will be presented and discussed. The behavior of the MOPA under continuous-wave (CW) conditions will first be presented for BAL bias currents at 0.95 I_{th} and 1.4 I_{th}, and the observations will be compared to the two-dimensional Fabry-Perot amplifier model and also to the one-dimensional gain model. The validity of each of these models will then be discussed.

The modulation characteristics of the MOPA configuration will then be presented. The small-signal AM frequency response data of the injected broad area laser will be presented for BAL bias currents at 0.95 I_{th} and 1.4 I_{th}, which are well characterized in the CW case. The frequency response data will include the magnitude and phase of the frequency response, along with the step impulse response calculated using the magnitude and phase response data. The effects of frequency modulation of the master oscillator will be considered in the analysis. The frequency response data will be compared to the current models of behavior for these devices which have been discussed previously.

The large-signal square-wave modulation response of the MOPA will then be presented for two modulation frequencies. Observations will be presented at the BAL bias currents of 0.95 Ith and 1.4 Ith. The square-wave modulation behavior will be compared with the small-signal frequency response analysis, and an evaluation of the modulated performance of the MOPA will be made.

3.2 CW Characteristics of the MOPA

The initial experiments were conducted with continuous-wave (cw) operation of the master oscillator. Data was collected for two bias levels of the BAL, $0.95I_{th}$ and $1.4I_{th}$, which resulted in free-running cw powers of 70 mW and 500 mW, respectively. The master oscillator was initially biased at $9.1I_{th}$, which resulted in 170 mW of CW output power from the laser. The frequency of the master oscillator was temperature-tuned for each BAL bias level until the wavelength of the master oscillator approximately matched the gain peak of the BAL, which occurs at 817 nm for $0.95\ I_{th}$ and 820 nm for $1.4\ I_{th}$. The spectrum of the master oscillator was observed to be single longitudinal mode, with no mode hops occuring over the temperature tuning range.

The master oscillator beam was aligned into the BAL, as discussed in Section 2.5. The injection position, angle, and frequency were all adjusted until the maximum amount of optical power in a single far-field lobe was obtained. The resulting far-field pattern of the BAL at $o.95\ I_{th}$ for end injection of the device at -5° is shown in Figure 3.1. The peak of the primary lobe is centered at +5° from the BAL facet normal, and the full-width half-maximum of the primary lobe is 0.12°. The amount of diffraction-limited power in the single lobe was measured to be 160 mW, which is over 90% of the total amplified power. The far-field pattern calculated using the two-dimensional Fabry-Perot Amplifier model discussed in Section 1.2 for the same conditions is shown in Figure 3.2; the angular position and width of the calculated lobe agrees well with the observation.

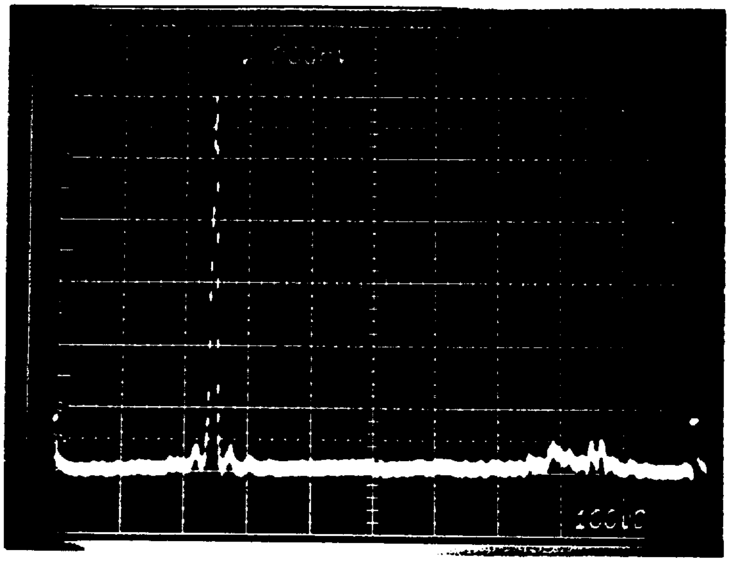

Figure 3.1 Measured far-field pattern of CW MOPA for BAL bias of 0.95 I_{th}; the injection angle is 4°, and the power in the single lobe is 160 mW (P_{inj} = 7.5 mW).

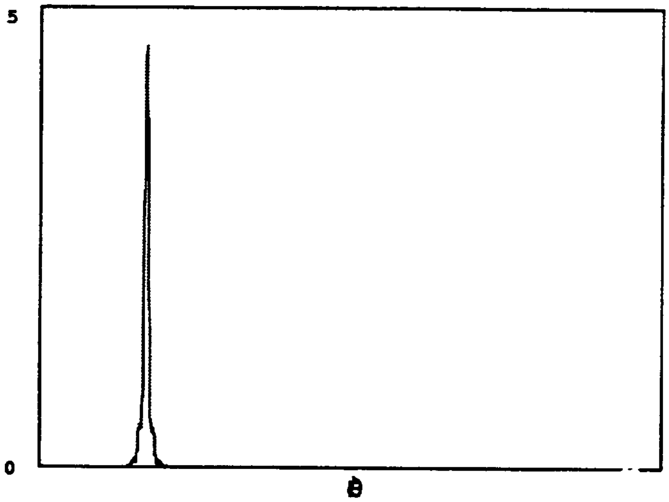

Figure 3.2 Calculated far-field pattern of MOPA from 2-D Fabry-Perot amplifier model, using injection angle of 4°.

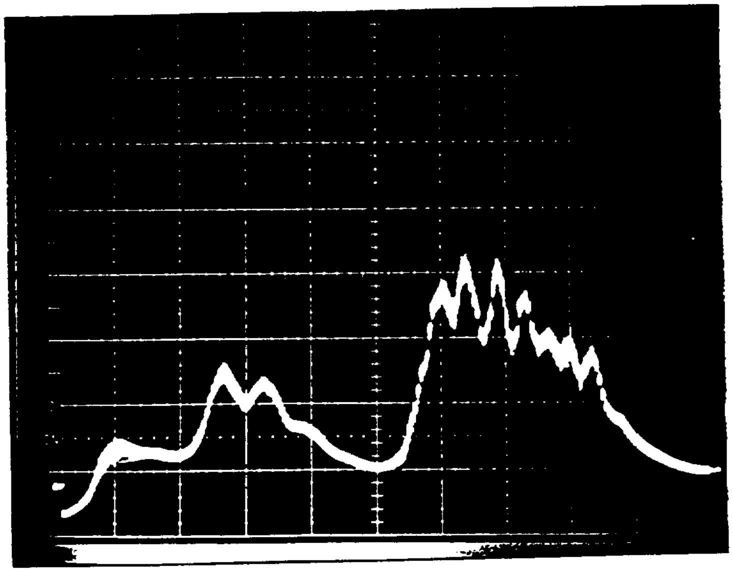

Figure 3.3 Measured near-field pattern of CW MOPA for BAL bias of 1.4 Ith; the injection angle is 5°, and the power in the single lobe is 340 mW (P_{inj}=10.4 mW).

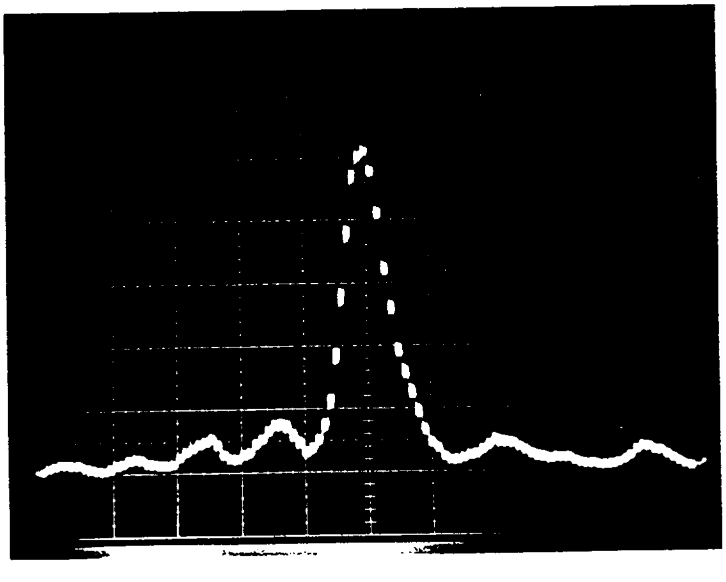

Figure 3.4 Measured far-field pattern of CW MOPA for BAL bias of 1.4 Ith; the injection angle is 5°, and the power in the single lobe is 340 mW (P_{inj}=10.4 mW).

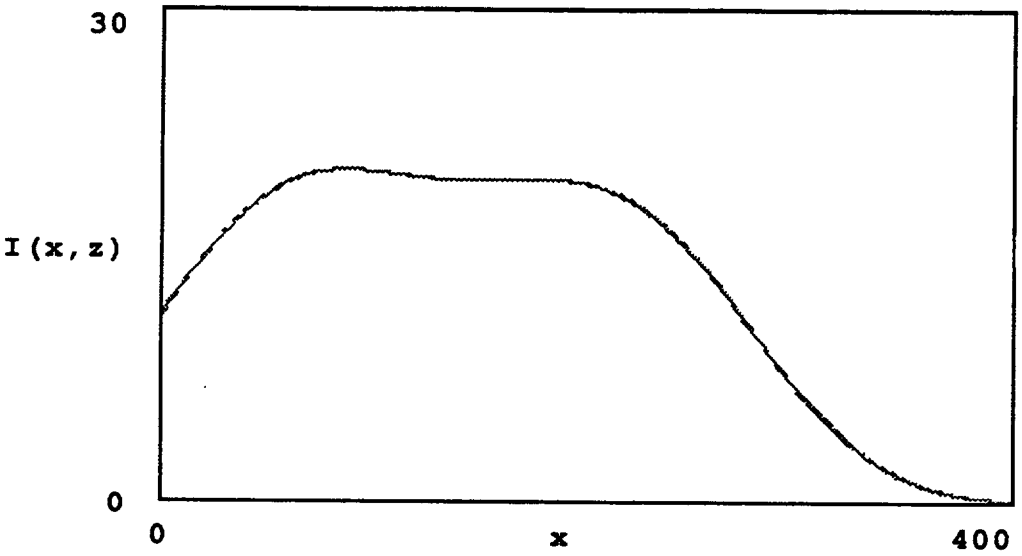

Figure 3.5 Calculated near-field pattern of MOPA for injection angle of 5°.

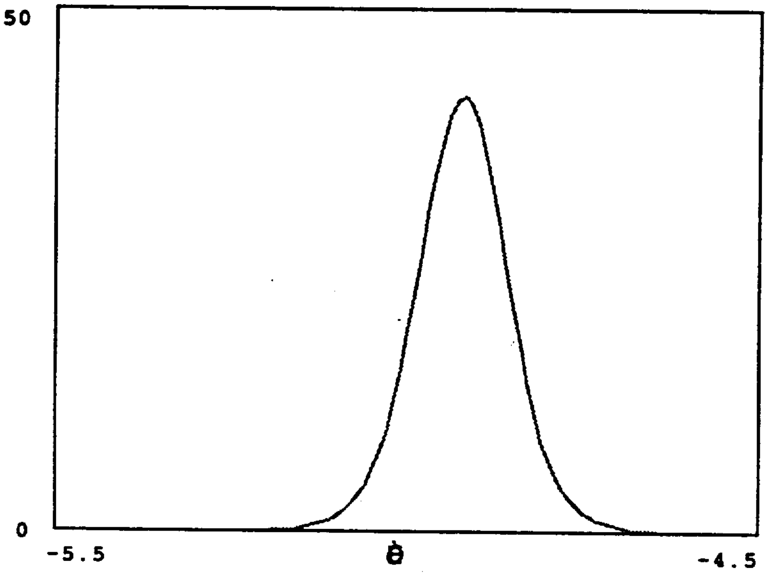

Figure 3.6 Calculated far-field pattern of MOPA for injection angle of 5°.

The measured near-field and far-field patterns of the MOPA for a BAL bias of $1.4I_{th}$ are shown in Figures 3.3 and 3.4, respectively. The power contained in the single lobe is 340 mW. The width of the central lobe has remained the same at 0.12°, but additional side lobes have appeared around the central lobe. The power in the side lobes is approximately 200 mW, making the percentage of total power in the single lobe is 63%. The corresponding calculated near-field and far-field patterns are given in Figures 3.5 and 3.6; again the agreement with the observed angular position and width of the central lobe is good, but the model does not account for the extraneous power in the side lobes. For both the 0.95 Ith and 1.4 Ith bias cases, it was determined that the angular positions of the side lobes correspond with those of the secondary maxima which would be formed by a plane wave diffracting through a 400 mm slit aperture. An increase in the amplitude of these side lobes indicates an increase in the wavefront errors, or spatial phase aberrations, in the internal propagating beam, causing more power to be diffracted into the secondary spatial lobes. The increase in the side lobe power observed for the high-gain case may then be due to phase aberrations caused by gain saturation, as discussed in Section 1.3, or may be caused by other processes that result in index inhomogeneities, such as thermal lensing. The magnitudes of these processes are the limiting factors for the maximum diffraction-limited output power that can be achieved from the MOPA.

The CW optical spectra of the MOPA beam at BAL bias currents of 0.95 Ith and 1.4 Ith are shown in Figures 3.7 and 3.8,

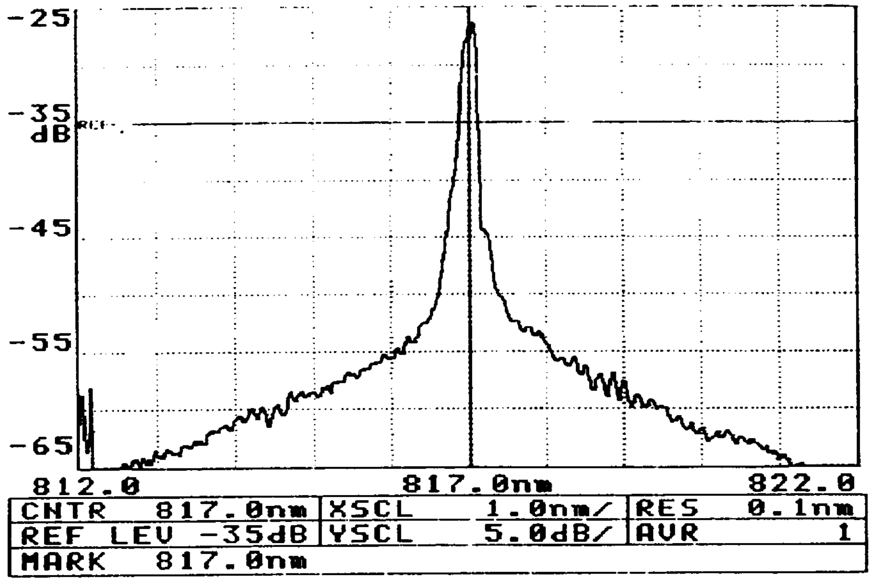

Figure 3.7: Optical Spectrum of CW MOPA for BAL bias of 0.95 Ith; the diffraction-limited power is 160 mW CW.

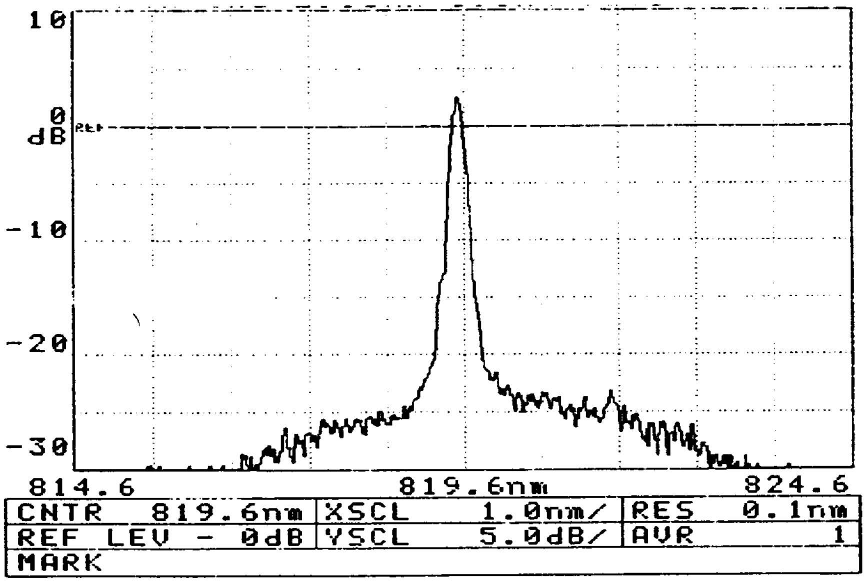

Figure 3.8: Optical spectrum of CW MOPA for BAL bias of 1.4 Ith; the diffraction-limited power is 340 mW CW.

respectively. The output is observed to be single longitudinal mode, at the same wavelength as the master oscillator. Using the optical spectrum analyzer, the suppression of the lower spectral modes was measured to be better than -20 dB.

The diffraction-limited output power and gain of the MOPA as a function of injected power were characterized using the variable neutral density filter and pinhole spatial filter as described in Section 2.5. The variable neutral density filter allowed for the attenuation of the injected beam without altering the wavelength (which is also a function of current). Any misalignment caused by the filter was readjusted to achieve the maximum amplitude of the primary lobe.

The diffraction-limited output power of the device as a function of injected power is shown in Figures 3.9 for BAL bias currents of 0.95 I_{th} and 1.4 I_{th}. The value for injected power considers all coupling losses into the device. The diffraction-limited gain derived from the data given in Figure 3.9 is shown in Figure 3.10, again for the two BAL bias levels.

For the case where BAL bias is below threshold current (0.95 I_{th}), the diffraction-limited output power is almost linear with injected power. The small-signal gain at this bias is 17 dB, which decreased by 3 dB at an injected power of 7.5 mW. The output intensity of the BAL at this point is 5 x 10^4W/cm^2 .If we consider this intensity to be the saturation output intensity I_{3dB}, then using Equation (1.32), we estimate the saturation intensity I_S to be approximately 7.5 x 10^4W/cm^2.

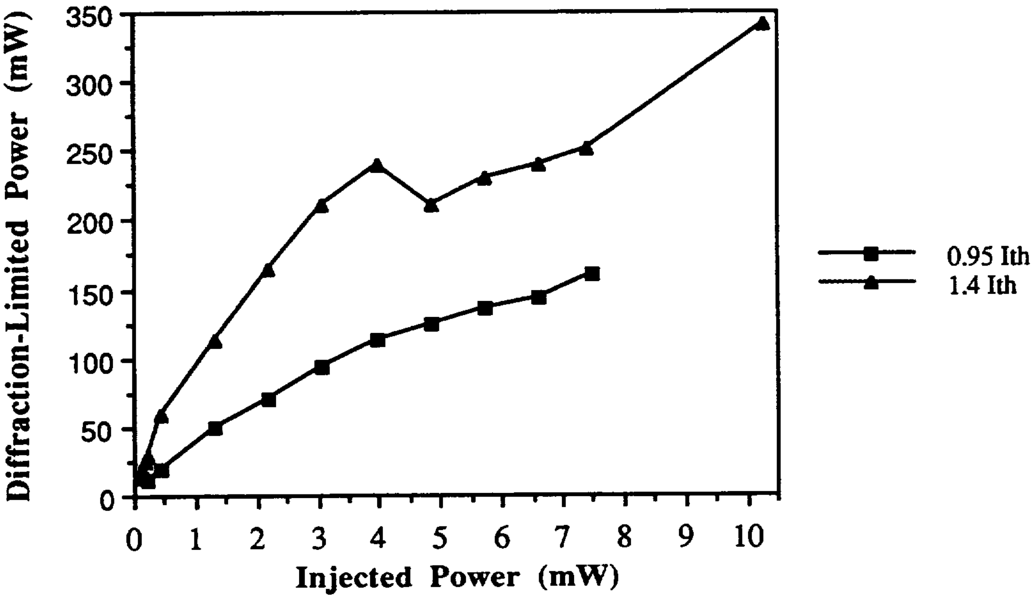

Figure 3.9: CW diffraction-limited power from MOPA as a function of injected power for BAL bias currents of 0.95 I_{th} and 1.4 I_{th}.

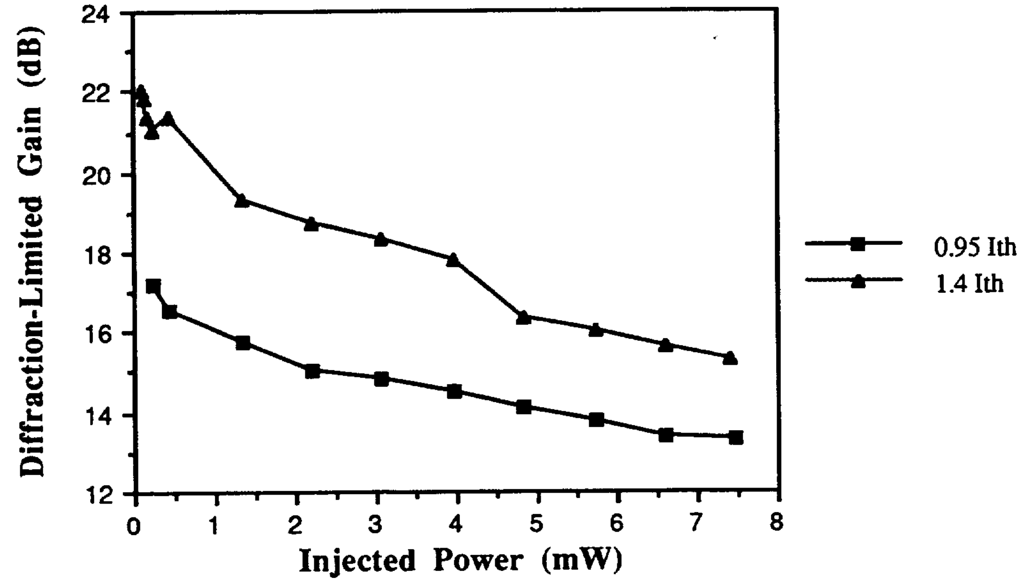

Figure 3.10: CW diffraction-limited gain versus injected power for BAL bias currents of 0.95 I_{th} and 1.4 I_{th}.

The diffraction-limited power for the case of 1.4 I_{th} BAL bias current also exhibits a saturated behavior, but with a discontinuity in the output power at 0.4 mW of injection, and again between 4 mW and 5 mW of injection. The gain between these injection levels is actually 1 dB higher than the other data points, as can be seen from Figure 3.9. The reason for this discontinuity is not known, but is probably due to spatial hole burning effects in the device. The small-signal gain is measured to be 22 dB, and using the same procedure as before, the experimentally-determined saturation intensity I_s is now approximately 5 x 10^4 W/cm^2. The strongly-saturated gain value is observed to be close to 15 dB, and the peak diffraction-limited power from the device is 340 mW.

The locking bandwidth of the MOPA was measured as a function of injected power, where the locking bandwidth is defined as the amount of master oscillator frequency detuning required to reduce the peak amplitude of the primary lobe by 3 dB. The lobe amplitude was monitored using the output of the 1024 x 1 CCD camera used to monitor the far-field pattern (see Section 2.6). The measured locking bandwidths for BAL bias currents of 0.95 I_{th} and 1.4 I_{th} are shown in Figure 3.11. The error in the measurement is ± 2 GHz.

The data reveals that the locking bandwidth of the MOPA increases with increasing injection power for both bias currents of the BAL; however, the locking bandwidth is larger when the BAL is biased at 0.95 I_{th}.

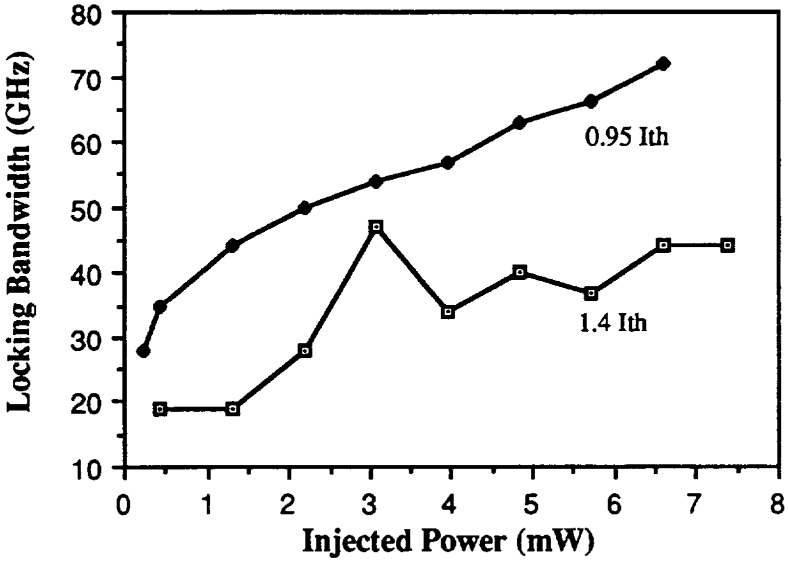

Figure 3.11: Locking bandwidth of primary spatial lobe as a function of injected power for BAL bias currents of 0.95 I_{th} and 1.4 I_{th} (Error is ± 2 GHz).

The locking bandwidth of the BAL for the given injection parameters was initially calculated using the two-dimensional Fabry-Perot amplifier model. The bandwidth value was determined to be 6 GHz, and is not a function of injected power. The calculated bandwidth is much less than the observed bandwidth, but it must be noted that the unity gain assumption limits the accurate modeling of the amplitudes of each of the passes. It is the summation of these amplitudes that define the half-power points of the locking bandwidth. The two-dimensional models which incorporate gain are better equiped to deal with this phenomena [25].

The one-dimensional reflective Fabry-Perot amplifier theory derived in Section 1.3 predicts a reduction in locking bandwidth with increasing gain, as shown in Figure 1.7. For small-signal gains of 17 dB and 22 dB (corresponding to BAL bias currents of 0.95 I_{th} and 1.4 I_{th}, respectively), the 3 dB bandwidths calculated from Equation (1.20) are 16 GHz and 10 GHz, respectively. Like the two-dimensional theory, the simplified 1-D Fabry-Perot gain model cannot make predictions about the bandwidth as a function of injected power, since it does not incorporate gain saturation. This leaves only one model which describes an increase of locking bandwidth with injection power; namely, the injection-locking model.

Under injection-locking theory, the locking bandwidth Δv_{lock} of the slave laser is given by [7]:

$$\Delta \upsilon_{lock} = \frac{1}{4\pi\tau_p}\sqrt{\frac{P_{in}}{P_{slave}}} \tag{3.1}$$

where P_{in} is the injected power, P_{slave} is the free-running power of the slave laser and τ_p is the photon lifetime of the cavity. The term before the square root is also known as the "cold cavity" bandwidth of the device, which is 75 GHz for the Fabry-Perot cavity. The calculated locking bandwidths for the two cases with 8 mW of injected power are 25 GHz and 10 GHz, where the slave laser powers are taken to be 70 mW (0.95 I_{th}) and 500 mW (1.4 I_{th}), respectively. These values are three times less than the measured bandwidths shown in Figure 3.11. We observe that the measured locking bandwidth is actually on the order of the cavity mode spacing, which is 75 GHz. By injection-locking theory, this result corresponds to the case where the injected power is on the order of the slave power. A closer examination of injection-locking theory is required.

The angular position of the single lobe was also observed to steer as a function of detuning the master oscillator frequency from the peak injected frequency. The primary lobe in the far-field was observed to steer at a linear rate of 1.6 x 10^{-2} degrees/GHz over the locking bandwidth, which did not vary as a function of injected power or BAL bias level. The 2-D Fabry-Perot amplifier model can be used to predict the angular tuning rate with frequency, since this should not depend on the relative amplitudes of the Gaussian beam passes. Running the 2-D amplifier model for the similar injection conditions yielded a calculated angular tuning rate of 1.6 x 10^{-2} degrees/GHz, which is in exact agreement with the experimental value.

Finally, it was observed that as the master oscillator frequency was detuned over the frequency spacing range of the Fabry-Perot resonances (75 GHz), another single lobed far-field pattern would be formed. The angular spacing of the lobes were observed to be 0.36°. The same effect was observed from calculations with the two-dimensional Fabry-Perot amplifier model, except that the angular spacing was a factor of 4 smaller. This discrepancy is not easily resolvable, since the angular position of the constructive interference pattern predicted by the 2-D FPA model should not be affected by the unity gain assumption for each pass.

From the CW observations of the injected BAL behavior, it appears that each of the models presented is not capable of describing the complete range of device behaviors. The two-dimensional Fabry-Perot amplifier model adequately models the far-field pattern, but does not reveal information about locking bandwidths or overall gain. The one-dimensional reflective Fabry-Perot model offers only a predicted locking bandwidth, but also does not deal with variations of this bandwidth as a function of injected power. The usefulness of this model will become apparent in the next section.

Finally, a case can be made from the observations for injection-locking, since the variation of locking bandwidth with power was observed to be linear, which is expected under this theory. Yet although the overall trends are right, the predicted locking bandwidth values are much smaller than the measured ones. A more detailed treatment of this theory should occur in our future work.

The CW observations to this point also allow us to predict that based on the measured locking bandwidth, a frequency chirp of the master oscillator up to 70 GHz for 8 mW of injected power should still result in the diffraction-limited output of at least half of the peak power value. The beam should also be observed to steer in time by 0.5°.

3.3 Modulated characteristics of the MOPA

3.3.1 Small-Signal AM/FM Frequency Response

The modulation characteristics of the MOPA configuration were initially characterized for a BAL bias current of 0.95 I_{th}. The frequency response of the BAL was measured for small-signal AM/FM modulation of the master oscillator, which has been previously characterized in Section 2.4. The frequency response characterization includes the amplitude response, phase response, and temporal step response of the system.

The experimental configuration for the measurement of the small-signal frequency response was discussed in Section 2.6.2 (see Figure 2.20). Prior to the frequency response measurements, the CW transmission characteristics of the spatial filter system (focusing lens and 25 mm pinhole) were determined as a function of the frequency injected into the BAL. The transmission versus detuning frequency is shown in Figure 3.12, where the BAL bias current is 0.95 I_{th} and the scale for the vertical axis is expressed as Power Down (dB).

This data reveals that the amplitude envelope of the single lobe as a function of injected frequency is asymmetrical. The locking bandwidth measured using the lens/pinhole spatial filtering system is 23 GHz, and the diffraction-limited power is observed to peak once again for a MO detuning of 75 GHz. This change in frequency corresponds exactly with the resonance frequency spacing of the Fabry-Perot cavity and also the previous CW data. The locking bandwidth of the BAL was similarly measured with the spatial filter, and the value was determined to be 13 GHz.

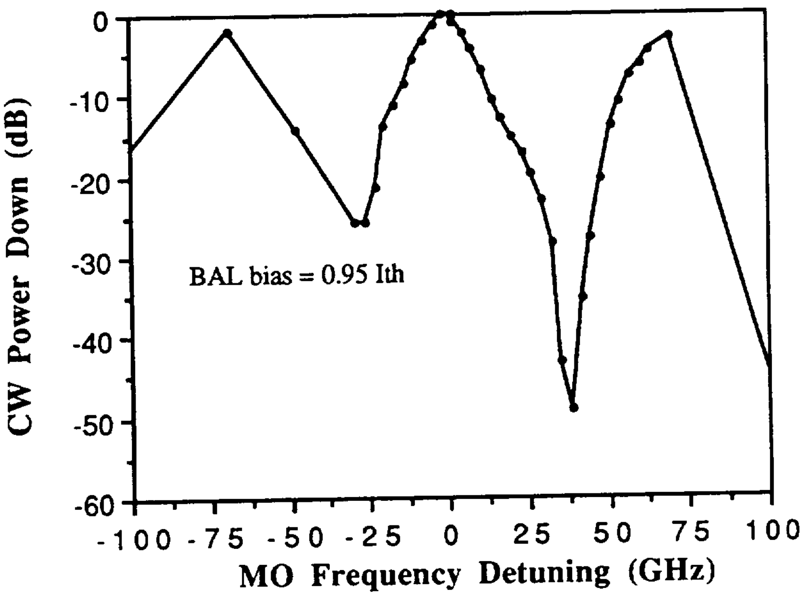

Figure 3.12:CW amplitude of primary lobe from MOPA as a function of MO frequency detuning from the peak value; the conditions are as shown in Figure 3.1 except that P_{inj} = 2 mW. The single lobe power is 65 mW CW.

It must be noted that the measured value for the locking bandwidth is less than the value of 47 GHz measured (for the same conditions) by monitoring the peak lobe amplitude on the 1024 x 1 CCD far-field camera. This discrepancy is a direct result of the optical system, as the beam is not perfectly collimated when it reaches the spatial filter. In a perfectly-collimated system, any beamsteering of the BAL single lobe would be translated into a lateral translation by the collimating optics. This lateral translation would again be converted to angular steering by the spatial filter system's focusing lens, which in turn focuses all angular rays to the same point in space, which in this case is the point in space where the pinhole is mounted. By this reasoning, for a perfectly-collimated beam, a small angular shift in a diffraction-limited beam from the BAL should be transmitted through the spatial filter (where small tilt aberrations have been neglected). The imperfect collimation of our beam was the primary motivation for the measurement of the transmission characteristics of the spatial filter system as a function of detuned MO frequency.

A 10 mA rms modulation current was applied to the MO (on top of the DC bias), so that the output of the MO was AM and FM modulated over an AM modulation frequency range from 300 KHz

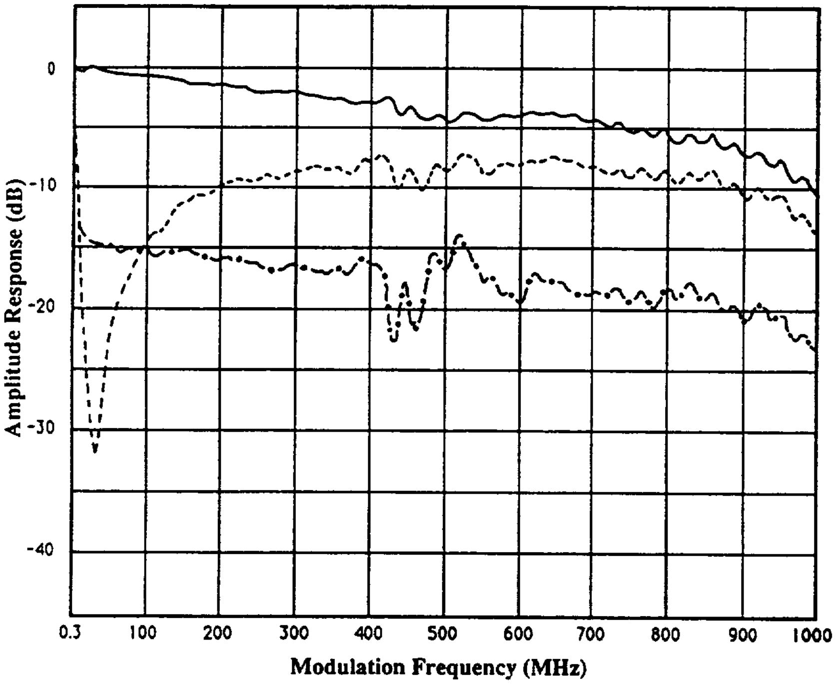

Figure 3.13: Amplitude of the 0.95 I_{th}-biased MOPA AM frequency response as a function of CW MO detuning for conditions given in text. Solid line: 0 GHz detuning, Dashed line: -9 GHz detuning, and Dotted line: -16 GHz detuning.

to 1 GHz. The AM/FM beam was injected into the BAL, and the ensuing amplitude response of the device was measured. The amplitude response of the MOPA is shown in Figure 3.13 as a function of CW frequency detuning of the master oscillator.

For no detuning of the MO frequency, the amplitude response is observed to be the same as that for the master oscillator alone (see Figure 2.4), which implies that the amplitude response of the BAL is essentially flat over this frequency range. This result agrees with a calculated bandwidth of the amplifier below threshold of 8 GHz.

The dashed line in Figure 3.13 denotes the amplitude response of the MOPA as the CW MO frequency is detuned by -9 GHz, which produces a CW reduction in response of -5 dB (see Figure 3.12). This CW drop in response is visible as an offset of the data; however, an additional drop in the response occurs from 0.3 MHz to 400 MHz, with a minimum response (27 dB down) occuring at 30 MHz. This drop in response is attributable to the FM modulation or frequency chirp of the MO, which was discussed in Section 1.4 and characterized in Section 2.4.2 (see Figure 2.10). The frequency chirp is effectively an increase in the detuning of the MO frequency from the BAL resonance peak, so the chirp tends to reduce the amplitude of the single-lobe, and therefore the amplitude response as seen by our measurement system.

The dotted line in Figure 3.13 represents the amplitude response for the case of -16 GHz of CW MO frequency detuning. The response appears to be similar to the response of the zero detuning case, except for an overall offset of the data of -15 dB. The CW amplitude response for this amount of detuning is -11 dB, as seen from Figure 3.12. The FM modulation does not appear to influence the amplitude response in this case.

The phase of the frequency response for the three detuning cases is shown in Figure 3.14. The phase response for the case of zero detuning (solid line) is observed to be close to 180°, which implies that the amplified BAL beam is in phase with the injected MO output (see Figure 2.5). As stated previously, the absolute phase shift of 180° is an artifact of the post-APD inverting amplifier; for discussion, we will consider only the relative phase shifts from this

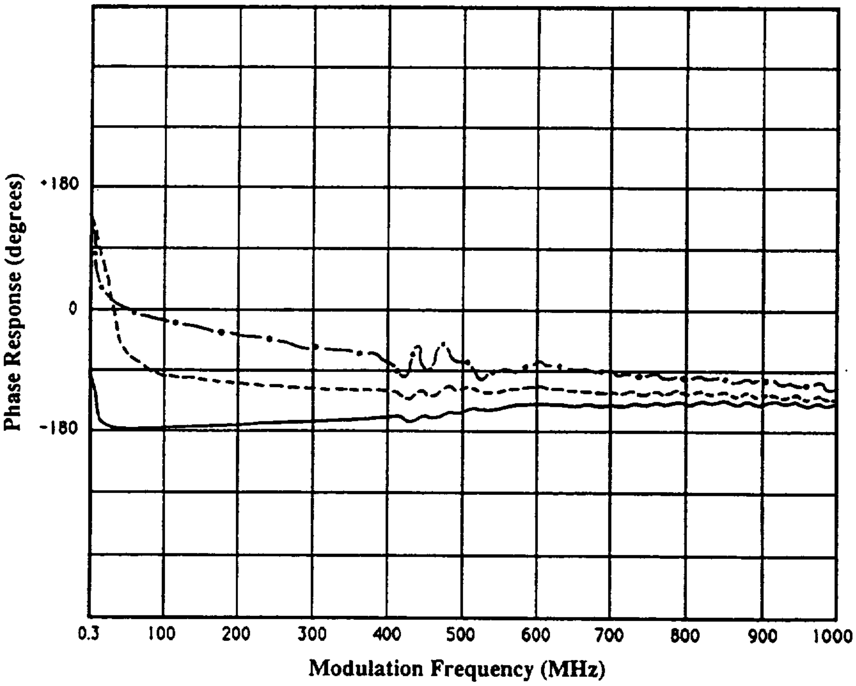

Figure 3.14: Phase of the 0.95 I_{th}-biased MOPA AM frequency response as a function of CW MO detuning for conditions given in text. Solid line: 0 GHz detuning, Dashed line: -9 GHz detuning, and Dotted line: -16 GHz detuning.

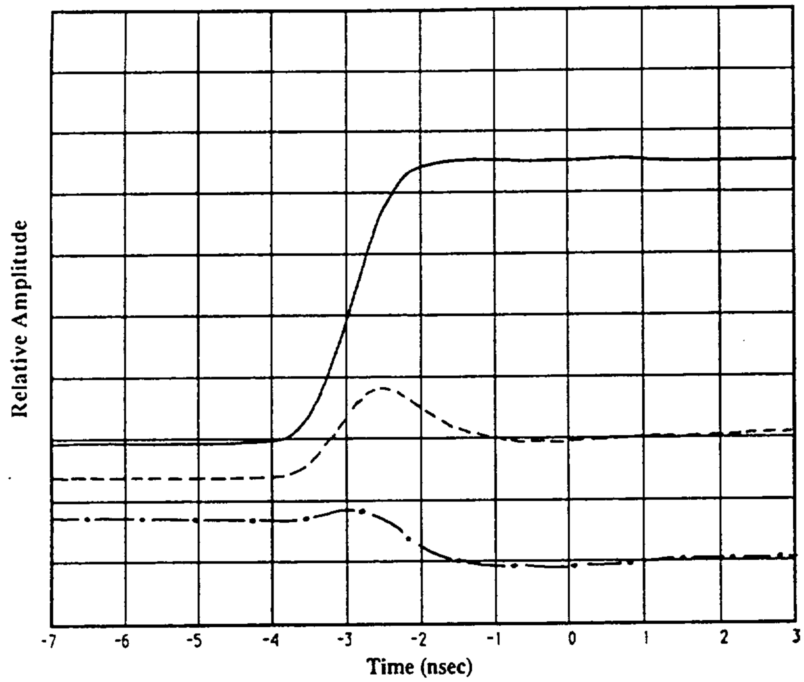

Figure 3.15: Calculated Step Response of the 0.95 I_{th}-biased MOPA from the AM frequency response as a function of CW MO detuning. Solid line: 0 GHz detuning, Dashed line: -9 GHz detuning, and Dotted line: -16 GHz detuning.

value, and round the phase shifts to the closest multiple of 90°. For frequency detuning of -9 GHz (dashed line), we see that the phase of the output begins at a 90° shift at low frequencies, then linearly increases to 270° shift, crossing the 180° shift point at 30 MHz, which also corresponds with the frequency of the minimum amplitude response. Similarly, the phase of the -16 GHz detuned signal (dotted line) begins around 90°, but the phase at higher frequencies remains closer to a 180° phase shift.

The effects of these observed phase shifts are manifest in the step response curves calculated from the amplitude and phase response information. Figure 13.15 shows these curves; for the case of no detuning (solid line), the step response of the MOPA output is similar to that of the MO source. For the case of -9 GHz detuning (dashed line), the direction of the step is the same, but the poor response of the BAL at low frequencies has caused the higher frequencies to dominate, resulting in a high-frequency peak at the start of the step. For the case of -16 GHz detuning, the phase has shifted by almost 180°, and the direction of the step has reversed to reflect this phase shift.

The bias current of the BAL was increased to a level of 1.4 Ith, where the device experiences self-oscillation under free-running conditions. The modulation of the master oscillator remained unchanged. The magnitude response, phase response and temporal step response measurements were each repeated for this BAL bias level; the results are given in Figures 3.16, 3.17, and 3.18, respectively. The behavior of the frequency response is strikingly similar to the observed behavior for the 0.95 I_{th} bias case, except that the amount of frequency detuning now required to reduce the magnitude response at low frequencies and shift the phase by -270° over most frequencies is now -3 GHz. At a detuning of -16 GHz, the magnitude of the response is on the same level as the zero detuning case, but the phase shift is almost exactly 180° over the modulation frequency range. The calculated step responses reflect these observations.

The effects of frequency chirp on the frequency response are most easily revealed from the phase of the frequency response data. Using the 1-D reflective Fabry-Perot amplifier model

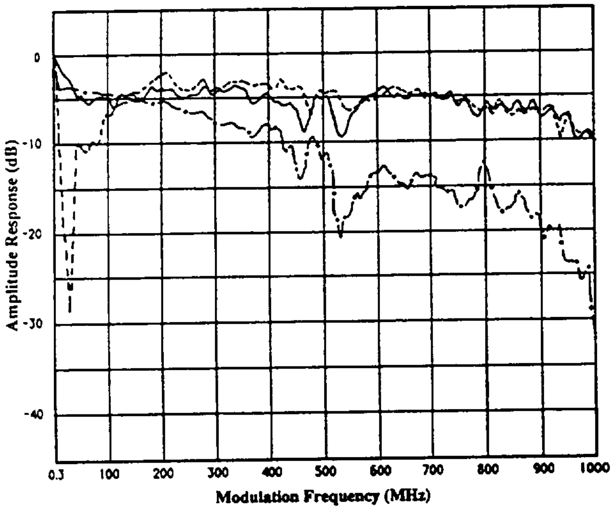

Figure 3.16: Magnitude of the 1.4 I_{th}-biased MOPA AM frequency response as a function of CW MO detuning for conditions given in text. Solid line: 0 GHz detuning, Dashed line: -3 GHz detuning, and Dotted line: -16 GHz detuning.

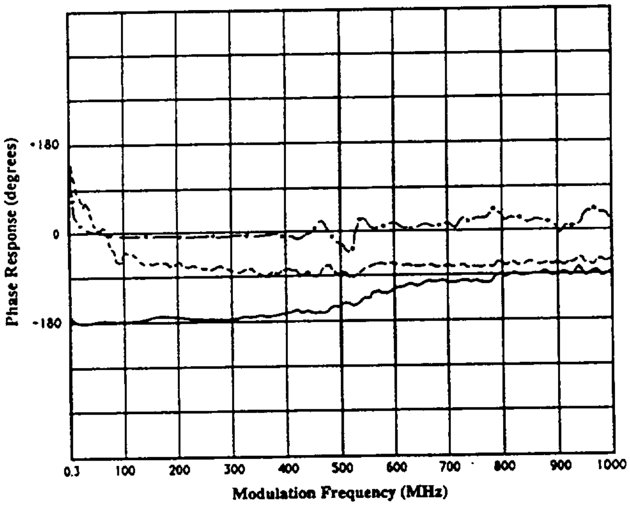

Figure 3.17: Phase of the 1.4 I_{th}-biased MOPA AM frequency response as a function of CW MO detuning for conditions given in text. Solid line: 0 GHz detuning, Dashed line: -3 GHz detuning, and Dotted line: -16 GHz detuning.

C-2

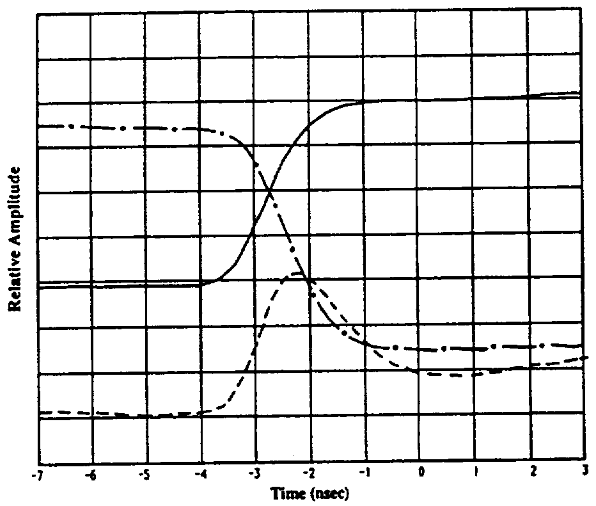

Figure 3.18: Calculated Step Response of the 1.4 I_{th}-biased MOPA from the AM frequency response as a function of CW MO detuning for conditions given in text. Solid line: 0 GHz detuning, Dashed line: -3 GHz detuning, and Dotted line: -16 GHz detuning.

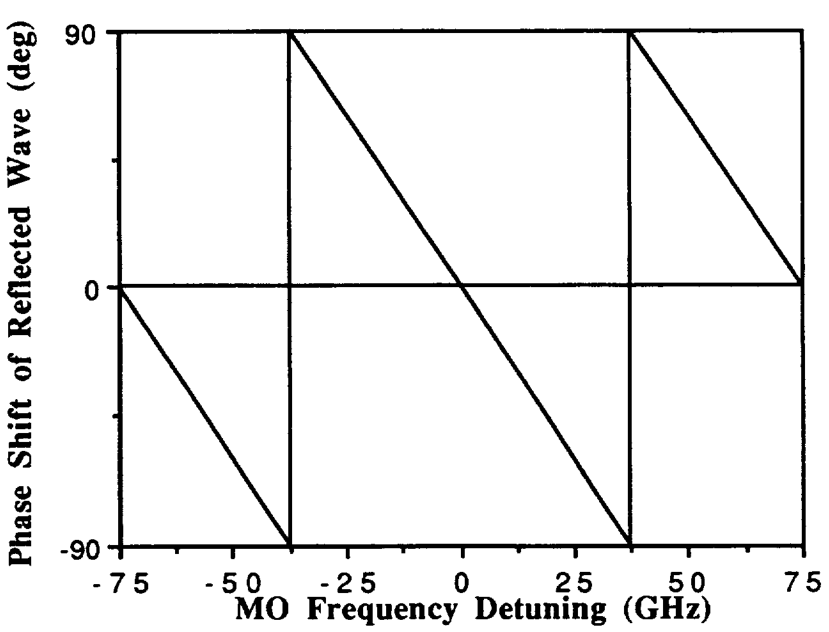

Figure 3.19: Calculated phase shift of reflected wave from 1-D Fabry-Perot amplifier using parameters in Table II (from Equation (1.19)).

of the BAL, we can calculated the phase shift of the reflected optical wave as compared to the incident optical wave, as shown in Figure 3.19. We see that the phase shift at the resonance frequency is zero, but increases or decreases almost linearly (due to the low front facet reflectivity) as the injected frequency is detuned from resonance. At the frequency midway between the resonances, the reflected phase experiences a discontinuity, shifting a total of 180°. The point can be viewed as a zero crossing on our phase response data, and corresponds to a minimum point in the reflected power. Hence, the magnitude of the frequency response should also be minimized at this frequency.

For the case where the BAL bias is 0.95 I_{th}, the measured locking bandwidth is 23 GHz, which must be noted to be only the frequency width of the gain peak. The absolute power minimum and phase discontinuity will occur at 37.5 GHz. From the data, we see that when the CW MO frequency is tuned to resonance, the FM modulation of the MO is not large enough to chirp the frequency past the 180° phase shift frequency. As the CW frequency of the master oscillator is detuned from resonance, the modulation frequencies with the highest amounts of FM modulation (which in this case is the low frequencies below 100 MHz) will be chirped past the phase discontinuity. For a CW frequency detuning which is close to the phase discontinuity point, the frequency modulation will chirp the laser across both sides of the discontinuity, resulting in a total phase shift during modulation of 180°. The same result is observed at the higher BAL bias point, but the locking bandwidth of the gain peak has been reduced. Note that the 180° phase shift in the frequency response data occurs for the same amount of detuning as in the low bias current case.

At this point, we must point out that the observed phase shift of the frequency response occurs at RF frequencies, and that the calculated phase shift of the reflected wave is at optical frequencies. Our observations imply that the phase shift imposed on the reflected optical wave is somehow transferred to the reflected RF wave. This observation can be explained by using the classical Drever-Hall configuration, as shown in Figure 3.20 [36].

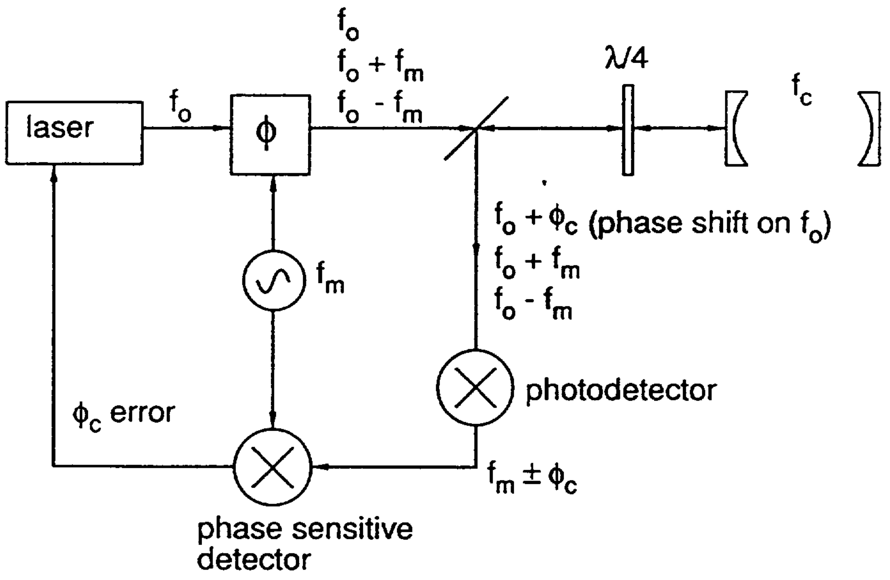

Figure 3.20: Classical Drever-Hall configuration for phase locking a laser to an external cavity.

In this configuration, the master oscillator is frequency-modulated at a frequency f_m, which results in sidebands centered around the carrier frequency f_0. This beam is reflected from a passive external cavity with resonant frequency f_c. The phase shift ϕ_c due to the frequency difference f_0-f_c is imparted to the reflected optical carrier frequency f_0, as we have demonstrated in Figure 3.19. The reflected optical beam then falls incident on a photodetector, which senses only the modulated frequency f_m and the superimposed phase shift ϕ_c. When the signal from the photodetector is mixed with the original modulation signal f_m, the residual phase shift ϕ_c can be detected. This phase shift can then be used to correct the initial phase of the master oscillator in a closed-feedback loop, and drive the phase difference between the master oscillator and the external cavity to zero. This technique is used to lock the frequency and phase of a laser to a resonance frequency of an external cavity.

By chance, the frequency response measurement system we have employed in conjunction with the MOPA configuration behaves exactly like the phase-detection portion of the Drever-Hall technique. In theory, we could actively lock the frequency and phase of our master oscillator to the peak resonances of the BAL by feeding the observed phase-shift back to our master oscillator. Our system would be limited to frequency modulations that remained in the locking bandwidth, while the presence of gain in the cavity will also present some problems (such as the phase shift caused by the gain itself).

3.3.2 Large-Signal Square-Wave Modulation Response

The large-signal square-wave response of the MOPA was also characterized at several modulation frequencies for BAL bias currents of 0.95 I_{th} and 1.4 I_{th}. The square-wave modulation signal was directly applied to the master oscillator, as described in Section 2.4.4. The measurement system used to characterize the large-signal square-wave behavior is discussed in Section 2.6.2.

The bias current of the injected BAL was initially set at 0.95 I_{th}, and the MO was biased to produce 2 mW of average injected power. When square-wave modulation was applied to the MO, the output beam varied from 4 mW peak to 0.2 mW, which corresponds to an extinction ratio of 15:1. The injection conditions for a 0.95 Ith BAL bias current are the same as those in Figure 3.1.

The optical waveform from the injected BAL for 10 MHz modulation is shown in Figure 3.21. The average peak power in the pulse is 80 mW, and the extinction ratio is approximately 12:1. The average diffraction-limited power in the pulse is 42 mW. The pulsewidth is 50 nsec, which corresponds to the injected pulsewidth, and the pulse exhibits a sharp increase at the leading edge, which is due to the presence of unsaturated gain.

The time-averaged far-field pattern of the pulsed output maintained the same angular position and width as the CW case, except that the peak amplitude had been reduced. It was also noted that the shape of the temporal waveform shown in Figure 3.21 varied as a function of pinhole position, indicating that beamsteering was occuring during the time of the pulses. The time-averaged

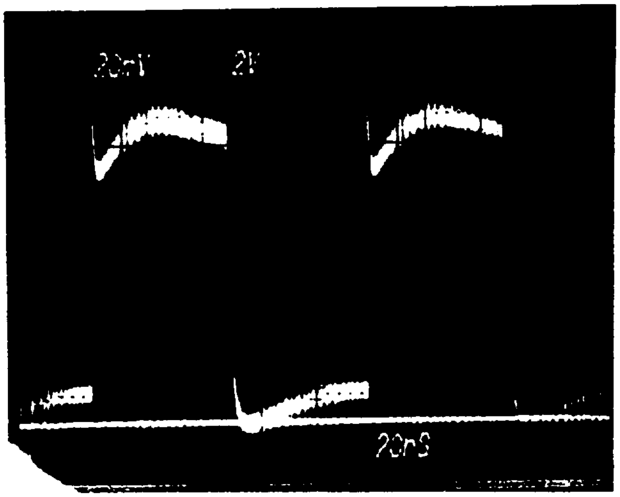

Figure 3.21: Optical waveform from 10 MHz square-wave modulated MOPA biased at 0.95 I_{th}. The diffraction-limited peak power is 80 mW (Pinj=2 mW average, 4 mW peak).

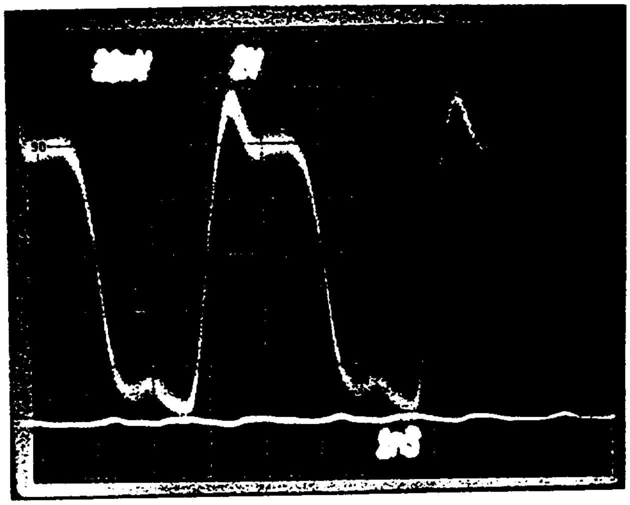

Figure 3.22: Optical waveform from 250 MHz square-wave modulated MOPA biased at 0.95 I_{th}. The diffraction-limited peak power is 120 mW (Pinj=2 mW average, 4 mW peak).

optical spectrum of the MOPA output was observed to be single-longitudinal mode.

The optical waveform from the injected BAL for 250 MHz modulation is shown in Figure 3.22. The average peak power in the pulse is now 120 mW, and the extinction ratio is approximately 12:1. The average diffraction-limited power in the pulse is 61 mW. The pulsewidth is now 2 nsec, which corresponds to the injected pulsewidth, and the pulse exhibits a sharp increase at the leading edge, which again is due to the presence of unsaturated gain.

The time-averaged far-field pattern of the pulsed output continued to maintained the same angular position and width as the 10 MHz and CW cases, except that the peak amplitude had now increased for the higher modulation frequency. Beamsteering was again observed during the time of the pulses, although the amount of beamsteering appeared to be reduced. The time-averaged optical spectrum of the MOPA continued to be single-longitudinal mode.

The bias of the BAL was increased to 1.4 Ith, but with the same operating conditions on the MO. For 10 MHz modulation, the time-averaged far-field conditions remained the same, but the amount of diffraction-limited average power increased to 100 mW. The peak power measured from the optical waveform was 200 mW, and the extinction ratio remained at 12:1. Beamsteering during the time of the pulses increased, as demonstrated in Figures 3.23 and 3.24, which show the optical output of the MOPA versus time as a function of the position of the spatial filter pinhole. The basic deduction from this observation is that our assumption of imperfect

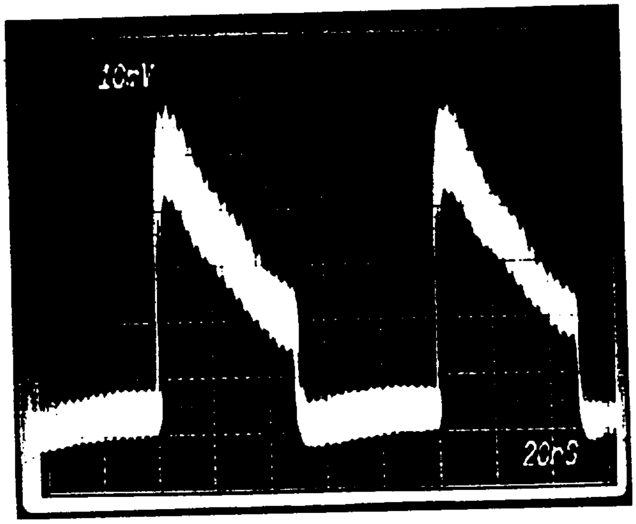

Figure 3.23: Optical waveform at one point in the far-field from 10 MHz square-wave modulated MOPA biased at 1.4 I_{th}. The diffraction-limited peak power is 200 mW (Pinj=2 mW average, 4 mW peak).

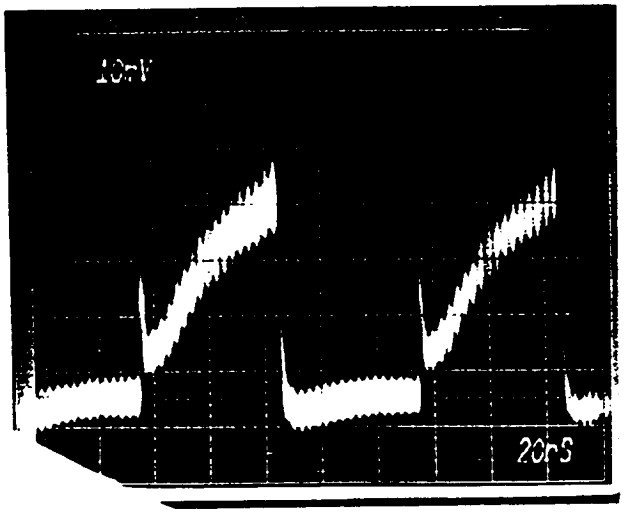

Figure 3.24: Optical waveform at another point in the far-field from 10 MHz square-wave modulated MOPA biased at 1.4 I_{th}. The diffraction-limited peak power is 200 mW (Pinj=2 mW average, 4 mW peak).

collimation is valid, and that an improved experiment to measure the time-resolved far-field pattern of the laser should be conducted.

The MOPA biased at 1.4 Ith was also injected with 250 MHz square-wave pulses. The time-averaged far-field pattern once again was single-lobed, but the average diffraction-limited power was now 120 mW. The optical waveform for this modulation rate was observed to be similar to the one observed previously, as shown in Figure 3.22.

The difference in average diffraction-limited power for the 10 MHz and 250 MHz modulation cases is directly attributable to frequency chirp. From the frequency chirp measurement of Section 2.4.2, we found that the frequency chirp at 250 MHz for 100 mA of modulation current is 4.5 GHz, which is well-within the locking bandwidth of the BAL. The frequency chirp at 10 MHz was not directly measureable, however, it must be extremely large, based on the small-signal frequency response data of the previous section. At the extreme values, the magnitude of this chirp is large enough to drive the BAL out of the locking bandwidth, leaving only the MO power "in-band" to be amplified.

Section 4: Conclusion

We have successfully demonstrated a semiconductor master oscillator-power amplifier using an AR-coated AlGaAs broad area laser as the amplifier. Under CW operating conditions, the device produced 340 mW of diffraction-limited, single-frequency optical power, with a locking bandwidth on the order of the resonant modes of the cavity. The locking bandwidth was determined to be a function of both the injected power and the bias of the device. The diffraction-limited lobe in the output was also observed to steer in angle as the frequency of the master oscillator was detuned from resonance. The small-signal gain of the device was measured to be 22 dB, while the strong-signal saturated gain was 15 dB.

The device was initially modeled in terms of multiple Gaussian beam propagation through a large Fabry-Perot cavity, which incorporates the both the longitudinal and transverse field behavior [8]. This model was found to be successful in describing the angular width, position, and steering of the primary lobe in the far-field, but did not successfully describe the locking bandwidth. The influence of injected power and amplifier bias on the locking bandwidth suggests a potential explanation using injection-locking theory [5]. This will be investigated further in the future. An additional model was developed for the device, based on a one-dimensional reflective Fabry-Perot cavity with gain. Saturation intensities for the device were measured using this model.

The frequency response of the master oscillator alone was found to be similar to that expected for a single-mode device, but the response rolled off sharply at 1 GHz due to the modulation electronics. The frequency chirp of the laser was also measured, although only for modulation rates above 100 MHz. When the response of the modulation electronics was compensated for, the values of the FM sensitivity as a function of modulation frequency basically agreed with previous measurements and also theory [9].

The frequency response of the MOPA was found to be a function of the frequency detuning of the master oscillator and the resonant amplifier. When the master oscillator frequency was tuned to resonance for the amplifier, the frequency and phase response replicated the response observed for the master oscillator alone. As the frequency of the MO was tuned away from resonance, the magnitude of the response experienced large drops at modulation frequencies where the frequency chirp was large. The phase of the response was also observed to shift linearly with the frequency deviation, making discontinuous shifts of 180° at frequencies corresponding to the anti-resonance frequencies of the amplifier. This phase shift at RF frequencies was attributed to the optical phase shift imparted to the beam reflected from the amplifier, as predicted by the one-dimensional reflective Fabry-Perot cavity model. The optical phase shift is imparted to the RF beam by frequency mixing. This phase shift has been used previously to frequency and phase-lock an oscillator to an external cavity in other laser systems [36]. We suggest that this technique may also be viable for locking the frequency and phase of the semiconductor master oscillator to the gain peaks of the resonant amplifier in the future.

Under square wave modulation, the MOPA was observed to produce 250 mW of diffraction-limited peak power at 250 MHz and 200 mW of diffraction-limited peak power at 10 MHz. The peak power for a given modulation frequency is basically determined by the injected power and the amplitude of the frequency chirp at this frequency. The ability of the MOPA to produce diffraction-limited high-power pulses at high modulation bandwidths encourages the pursuit of further research on this system in the future.

References

[1] R. Solarz, "High Power Diode Laser Arrays," *IEEE/LEOS Annual Meeting*, San Jose, CA, Nov. 4-7, 1991.

[2] L. Goldberg and M.K. Chun, "Injection locking characteristics of a 1 Watt broad stripe laser diode," Applied Physics Letters, vol. 50, pp. 1900-1902, 1988.

[3] L. Goldberg, H.F. Taylor, J.F. Weller, and D.R. Scifres, "Injection locking of coupled-stripe diode laser arrays," Applied Physics Letters, vol. 46, pp. 236-238,1985.

[4] J.P. Hohimer, A. Owyoung, and G.R. Hadley,"Single-channel injection locking of a diode-laser array with a CW dye laser," Applied Physics Letters, vol. 47, pp. 1244-1246,1985.

[5] R. Adler, " A study of locking phenomena in oscillators," Proceedings of the IRE, vol. 34, pp. 351-357, 1946.

[6] H.L.Stover and W.H. Steier, "Locking of laser oscillators by light injection," Applied Physics Letters, vol. 8, pp. 91-93, 1966.

[7] S. Kobayashi and T. Kimura, "Injection locking in AlGaAs semiconductor laser," IEEE Journal of Quantum Electronics, vol. QE-17, pp. 681-689, 1981.

[8] G.L. Abbas, S. Yang, V.W.S. Chan, and J.G. Fujimoto, "Injection behavior and modeling of 100 mW broad area diode lasers," IEEE Journal of Quantum Electronics, vol. 24, pp. 609-616,1988.

[9] S. Kobayashi, et al., "Direct frequency modulation in AlGaAs semiconductor lasers," IEEE Journal of Quantum Electronics, vol. QE-18, pp. 582-595, 1982.

[10] D.F. Welch, W. Streifer, and D.R. Scifres, "High power single-mode diode lasers," Proceedings of SPIE, vol. 1043, p. 54-60, 1989.

[11] J.C. Simon, "Semiconductor laser amplifier for single mode optical fiber communications," Journal of Optical Communications, vol. 4, pp. 51-62, 1983.

[12] T. Mukai and Y. Yamamoto, "Gain, frequency bandwidth, and saturation output power of AlGaAs DH Laser Amplifiers, IEEE Journal of Quantum Electronics, vol. QE-17, pp. 1028-1034, 1981.

[13] A. J. Lowery, "A new dynamic semiconductor laser model based on the transmission line modelling method," IEE Proceedings Journal of Optoelectronics, vol. 134, pp. 281-289, 1987.

[14] A.A.M. Saleh, "Non-linear models of travelling wave laser amplifiers," Electronics Letters, vol. 24, pp. 835-837, 1988.

[15] G. Eisenstein, "Semiconductor Optical Amplifiers," IEEE Circuits and Devices, vol 5, pp. 25-30, July1989.

[16] A.J. Collar, et al., "Fabrication and performance of $\lambda=1.5$ μm angled facet laser amplifiers," in *Technical Digest of the 11th IEEE International Semiconductor Laser Conference* (Boston, MA), 1988, Postdeadline paper 6.

[17] J.R. Andrews, "Traveling wave amplifier made from a laser diode array," Applied Physics Letters, vol. 48, pp. 1331-1333, 1986.

[18] L.Y. Pang, E.S. Kintzer, and J.G. Fujimoto,"Two-stage injection locking of high-power semiconductor arrays," Optics Letters, vol. 15, pp. 728-730, July 1990.

[19] L. Goldberg and J. F. Weller, "Broad-area high-power semiconductor optical amplifier," Applied Physics Letters, vol. 58, pp. 1357-1359, 1991.

[20] L. Goldberg, et al., "12 W broad area semiconductor amplifier with diffraction-limited optical output," Electronics Letters, vol. 27, pp. 927-929, 1991.

[21] J.K. Butler, et al., "Coupled mode analysis of phase-locked injection laser arrays," Applied Physics Letters, vol. 44, pp. 293-295, 1984.

[22] G.R. Hadley, et al., "Modeling of injection-locking phenomena in diode laser arrays," Optics Letters, vol. 11, pp. 144-146, 1986.

[23] J.M. Verdiell, R. Frey, and J.P. Huignard, "Analysis of Injection-Locked Gain-Guided Diode Laser Arrays," IEEE Journal of Quantum Electronics, vol. 27, pp. 396-401,1991.

[24] M.K. Chun, L. Goldberg, and J.F. Weller, "Injection-beam parameter optimization of an injection-locked laser diode array," Optics Letters, vol. 14, pp. 272-274, 1989.

[25] G.C. Dente and M.L. Tilton, "Modelling broad-area semiconductor optical amplifiers," to be published in IEEE Journal of Quantum Electronics, 1991.

[26] L. Goldberg, et al., "Frequency modulation characteristics of coupled-stripe laser diode array," IEEE Journal of Quantum Electronics, vol. QE-22, pp. 513-516, 1986.

[27] E.A. Swanson, et al., "High-speed electronic beamsteering using injection locking of a laser-diode array," Optics Letters, vol. 12, pp. 30-32, 1987.

[28] M. Lucente, et al., "Coherent optical communication with injection-locked high-power semiconductor laser array," Electronics Letters, vol. 25, pp. 1112-1113, 1989.

[29] J.C. Livas, et al., "1 Gbit/s injection-locked DPSK communications experiments for space applications," Electronics Letters, vol. 27, pp. 123-125 , 1991.

[30] A. Siegman, Lasers, pp. 450, 1986.

[31] T. Saitoh and T. Mukai, "Gain saturation characteristics of traveling-wave semiconductor laser amplifiers in short optical pulse amplification," IEEE Journal of Quantum Electronics, vol. QE-26, pp. 2086-2094, 1990.

[32] L.M. Frantz and J.S. Nodvik, "Theory of pulse propagation in a laser amplifier," Journal of Applied Physics, vol. 34, pp. 2346-2349, 1963.

[33] A. Yariv, Optical Electronics, pg. 491, 1985.

[34] D. Welford and S.B. Alexander, "Magnitude and phase characteristics of frequency modulation in directly modulated AlGaAs semiconductor diode lasers," IEEE Journal of Lightwave Technology, vol. LT-3, pp. 1192-1199, 1985.

[35] A. Yariv, Quantum Electronics, pg. 263, 1989.

[36] R. Drever, J. Hall, and F. Kowalski, "Laser phase and frequency stabilization using an optical resonator," Applied Physics B, vol. 31, pp. 97-105, 1983.

[37] M.J. Adams, H.J. Westlake, M.J. O'Mahony, and I.D. Henning, " A comparison of active and passive bistability in semiconductors," IEEE Journal of Quantum Electronics, vol. QE-21, 1985.

[38] M. Dagenais, Z. Pan, T.N. Ding, and H. Lin, "Diode laser based optical logic devices," SPIE Digital Optical Computing, vol. CR35, pp. 126-154, 1990.

REPORT DOCUMENTATION PAGE

Form Approved
OMB No. 0704-0188

1. AGENCY USE ONLY *(Leave blank)*

2. REPORT DATE
November 1992

3. REPORT TYPE AND DATES COVERED
Technical Memorandum

4. TITLE AND SUBTITLE
Modulation Characteristics of a High-Power Semiconductor Master Oscillator Power Amplifier (MOPA)

5. FUNDING NUMBERS
710

6. AUTHOR(S)
Donald Mitchell Cornwell, Jr.

7. PERFORMING ORGANIZATION NAME(S) AND ADDRESS(ES)
Space Technology Division
Goddard Space Flight Center
Greenbelt, Maryland 20771

8. PERFORMING ORGANIZATION REPORT NUMBER
93B00016

9. SPONSORING/MONITORING AGENCY NAME(S) AND ADDRESS(ES)
National Aeronautics and Space Administration
Washington, D.C. 20546-0001

10. SPONSORING/MONITORING AGENCY REPORT NUMBER
TM-104577

11. SUPPLEMENTARY NOTES

12a. DISTRIBUTION/AVAILABILITY STATEMENT
Unclassified - Unlimited
Subject Category 33

12b. DISTRIBUTION CODE

13. ABSTRACT *(Maximum 200 words)*

A semiconductor master oscillator-power amplifier was demonstrated using an anti-reflection (AR) coated broad area laser as the amplifier. Under CW operation, diffraction-limited single-longitudinal-mode powers up to 340 mW were demonstrated. The characteristics of the far-field pattern were measured and compared to a two-dimensional reflective Fabry-Perot amplifier model of the device. The MOPA configuration was modulated by the master oscillator. Prior to injection into the amplifier, the amplitude and frequency modulation properties of the master oscillator were characterized.
The frequency response of the MOPA configuration was characterized for an AM/FM modulated injection beam, and was found to be a function of the frequency detuning between the master oscillator and the resonant amplifier. A shift in the phase was also observed as a function of frequency detuning; this phase shift is attributed to the optical phase shift imparted to a wave reflected from a Fabry-Perot cavity. Square-wave optical pulses were generated at 10 MHz and 250 MHz with diffraction-limited peak powers of 200 mW and 250 mW. The peak power for a given modulation frequency is found to be limited by the injected power and the FM modulation at that frequency. The modulation results make the MOPA attractive for use as a transmitter source in applications such as free-space communications and ranging/altimetry.

14. SUBJECT TERMS
Power Amplifier, Power Modulation, Master Oscillator, Electronics,
AM/FM Frequency

15. NUMBER OF PAGES
110

16. PRICE CODE

17. SECURITY CLASSIFICATION OF REPORT
Unclassified

18. SECURITY CLASSIFICATION OF THIS PAGE
Unclassified

19. SECURITY CLASSIFICATION OF ABSTRACT
Unclassified

20. LIMITATION OF ABSTRACT
Unlimited

NSN 7540-01-280-5500

Standard Form 298 (Rev. 2-89)
Prescribed by ANSI Std. 239-18, 298-102